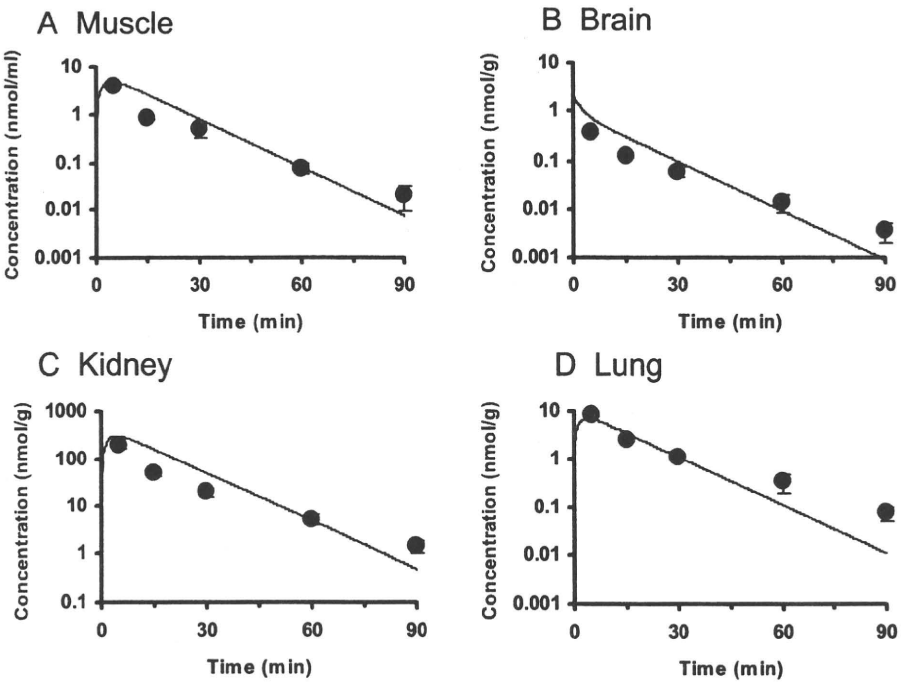

Fig. 5. Simulated and observed tissue concentration profiles for pravastatin in rats after intravenous administration at 10 mg/kg. Symbols and solid lines, experimentally observed and simulated values, respectively. Each point represents the mean ± S.E. (n = 3).

even under nonlinear conditions (200 mg/kg) (Fig. 4). These results suggest that the PBPK model constructed in this study is appropriate for describing the pharmacokinetics of pravastatin in rats.

The kinetic parameters PS_{inf}, PS_{dif}, and PS_{bile} were also determined in vitro using rat hepatocytes and CMVs to obtain the relevant SFs (Table 2). The corresponding parameters were also determined using human cryopreserved hepatocytes and CMVs. These parameters were extrapolated in vivo using the SFs determined in rats. Because there is no evidence that active transport mechanisms are involved in the sinusoidal efflux of pravastatin, the clearance corresponding to the nonsaturable component (PS_{dif}) of the uptake was used as the clearance for sinusoidal efflux. Unlike the rat liver S9 fractions, pravastatin was not metabolized in the human liver S9 fractions. Therefore, the metabolic clearance was set to zero in humans. Using the human parameters, simulated plasma concentration-time profiles of pravastatin after the intravenous and oral administration were fairly close to the observed data for humans (Fig. 6), showing that the predicted value was not far from the true value. It should be noted that the sinusoidal efflux clearance (passive diffusion clearance) was lower than the intrinsic biliary clearance with regard to the liver concentration, indicating that the hepatobiliary transport of pravastatin is likely uptake limited and that the hepatic intrinsic clearance can be approximated to PS_{inf} (Shitara et al., 2006a). Therefore, even though the predictability of the absolute values for biliary and sinusoidal efflux clearance is low, the simulated results will be close to the observed data as far as the uptake clearance is correctly predicted. To validate the predictability of those clearances, the liver concentrations must be determined in humans, which should be possible with imaging technologies such as positron emission tomography, single-photon emission computed tomography, and magnetic resonance imaging. Ghibellini et al. (2007) recently developed a methodology for the real-time measurement of the biliary excretion profiles of drugs in humans using a gamma scintigraphy technique. Further efforts are required to use such in vivo imaging technologies to increase the predictability of these pharmacokinetic parameters.

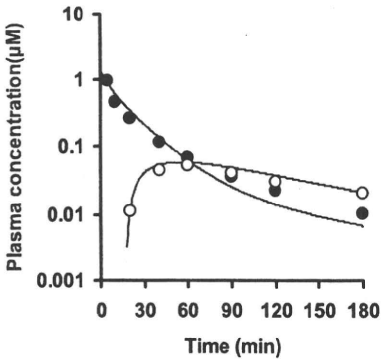

Fig. 6. Predicted and observed plasma concentration profiles for pravastatin in humans. Closed and open symbols, reported plasma concentrations after intravenous (9.9 mg) and oral (19.2 mg) administration, respectively (Singhvi et al., 1990). Solid lines, simulated values using the parameters shown in Tables 1 and 2.

To date, clinical studies have demonstrated that the genetic variations of OATP1B1 and drug-drug interactions involving OATP1B1 are associated with interindividual differences in the systemic exposure of pravastatin and other substrate drugs (Nishizato et al., 2003; Maeda et al., 2006; Niemi et al., 2006; Shitara and Sugiyama, 2006b). Because the pharmacological target of pravastatin is inside the cell, the liver exposure is a critical factor for its pharmacological activities. Based on the pharmacokinetic concepts, the AUC in the liver concentration is governed only by the sequestration clearance from the liver as far as the renal elimination is

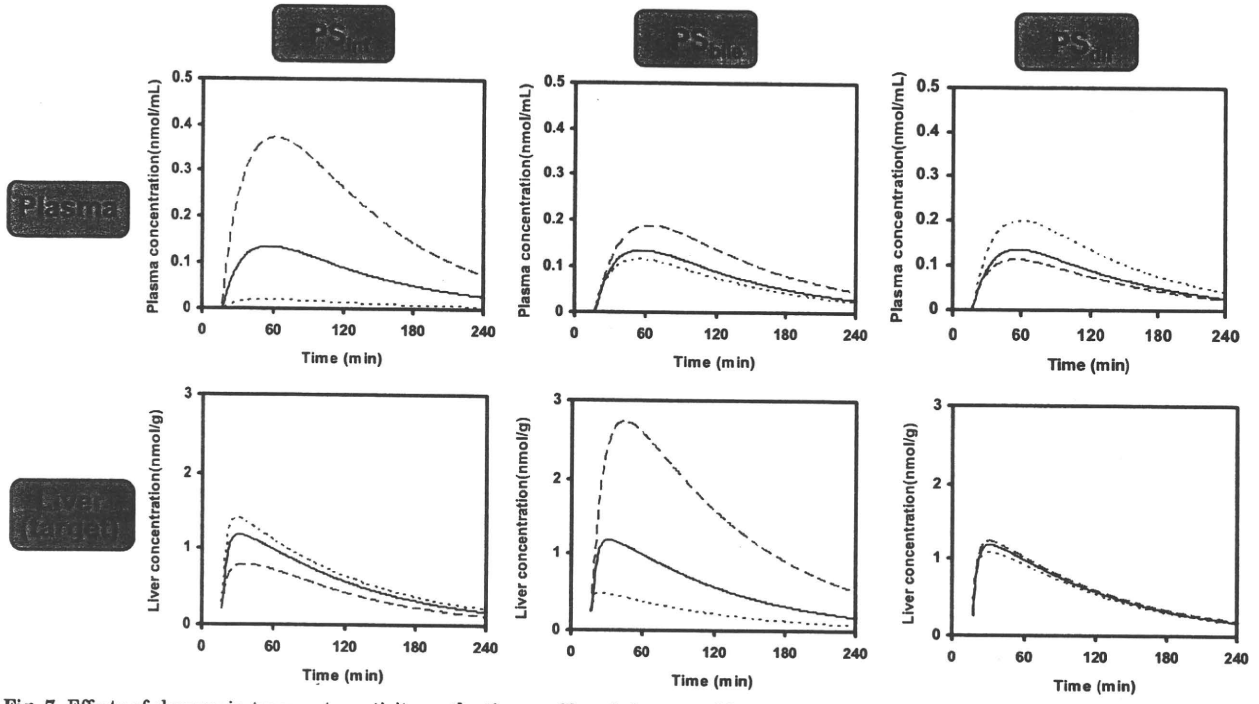

Fig. 7. Effects of changes in transporter activity on the time profiles of plasma and liver (target organ) concentrations of pravastatin in humans. Plasma and liver concentrations after oral administration (40 mg) were simulated using the PBPK model with varying hepatic transport activities over a 1/3- to 3-fold range of the initial values shown in Table 1. (———, initial; – – –, ×1/3; · · · · · · · · ·, ×3)

negligible and is independent of the change in uptake clearance (eq. A4) (see Appendix II). When renal clearance makes a significant contribution, the changes in hepatic uptake activity can affect both the liver and the plasma AUC (Fig. 9; Appendix II). Actually, the renal elimination of pravastatin makes a significant contribution to the total body clearance (47% of the total body clearance) (Singhvi et al., 1990). Therefore, it is possible that the liver concentrations of pravastatin are affected to some extent also by the changes in the hepatic uptake activity. To support this concept, a simulation was performed with different uptake clearances (Fig. 7). Changes in the hepatic uptake clearance had a great impact on the plasma concentrations of pravastatin but less impact on the liver concentrations. In accordance, the effects of the genetic polymorphisms of OATP1B1 on the cholesterol-lowering effects of pravastatin will be small or absent at least at steady state (in other words, after relatively long-term treatment). The alteration of pharmacological effect of pravastatin with its chronic administration has not been observed in subjects with OATP1B1 polymorphisms although alteration of inhibitory effect of HMG CoA reductase activities in short-term treatments was reported (Takane et al., 2006; Kivistö and Niemi, 2007; Zhang et al., 2007). In contrast, changes in the intrinsic canalicular efflux activity should dramatically affect the liver concentration of pravastatin, whereas the plasma concentration is not affected as much by changes in the intrinsic biliary clearance (Fig. 7). Because the biliary excretion of pravastatin is mainly mediated by MRP2, the factors affecting MRP2 function, such as the use of MRP2 inhibitors or the genetic mutations causing Dubin-Johnson syndrome, will affect the pharmacological action of pravastatin. Furthermore, changes in the sinusoidal efflux clearance had only a slight impact on both the plasma and the liver concentrations. This is because, even under these conditions, the uptake process is still the rate-limiting process. Although the predictability of the sinusoidal efflux clearance remains unknown, changes within this range will not affect the simulated results.

TABLE 3

Changes in the AUC (percentage of the control) for plasma and liver concentrations of pravastatin after its oral administration when the transporter function changes

Change in Clearance	PS_{inf}		PS_{bile}		PS_{dif}	
	Plasma	Liver	Plasma	Liver	Plasma	Liver
×1	100	100	100	100	100	100
×1/3	271	68	143	255	83	103
×3	14	115	84	38	146	92

One of the serious adverse effects of statins is myopathy (rhabdomyolysis). Because its target organ is the skeletal muscle, the systemic exposure should be the determinant factor of this adverse effect. The sensitivity analyses showed that the changes in the hepatic uptake clearance had a great impact on the systemic exposure of pravastatin, whereas those in the canalicular efflux had a minimal impact (Fig. 7). The results suggest that patients with an impaired OATP1B1 might be more susceptible to pravastatin-induced myopathy than those with normal one. Morimoto et al. (2004) reported that the frequency of the OATP1B1*15 haplotype was significantly higher in patients who experienced myopathy after receiving pravastatin or atorvastatin (which is also an OATP1B1 substrate) than in patients without myopathy, and a genome-wide study elucidated that the variants in OATP1B1 are strongly associated with an increased risk of simvastatin-induced myopathy (Link et al., 2008).

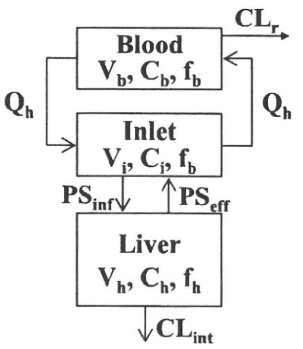

Fig. 8. Simple model to analyze the effects of changes in hepatic uptake activity and intrinsic clearance on blood and liver concentrations. Indicated are the hepatic blood flow (Q_h), renal clearance (CL_r), volume (V), concentration (C), unbound fraction (f), hepatic uptake clearance (PS_{inf}), sinusoidal efflux clearance (PS_{eff}), intrinsic clearance (CL_{int}), blood (b), inlet (i), and liver (h).

In the present study, a PBPK model, including transporter-mediated membrane transport processes, was constructed, which allows the prediction of the pharmacokinetics of pravastatin in humans. It also extends our understanding of the effects of changes in the transport processes on the pharmacological and adverse effects of drugs by simulating the exposure of the systemic circulation and tissues to them. The present study suggests that changes in the OATP1B1 activities may have a small and a large impact on the therapeutic efficacy and side effect (myopathy) of pravastatin, respectively, whereas those in the MRP2 activities may have opposite impacts (i.e., a large and a small impact on the therapeutic efficacy and side effect).

Appendix I: Differential Mass Balance Equations for the PBPK Model

Nomenclature

General. Q, blood flow rate; V, tissue weight; C, pravastatin concentration; K_p, tissue/blood partition coefficient; f_B, blood unbound fraction; f_T, tissue unbound fraction; V_m, maximum transport velocity; K_m, half-saturation concentration for transport; CL_R, renal clearance; PS_{inf}, intrinsic hepatic uptake clearance; PS_{dif}, passive diffusion clearance on the sinusoidal membrane; PS_{bile}, intrinsic biliary clearance; CL_{met}, intrinsic metabolic clearance; Fa, fraction absorbed; k_a, absorption rate constant.

Subscripts. B, blood; LU, lung; BR, brain; MU, muscle; R, kidney; GI, gastrointestinal tract; H, liver; HE, liver extracellular space; inf, influx; met, metabolism.

Model Equations

Hepatic uptake, biliary excretion, and metabolic clearances in humans were linear parameters.

Blood pool:

$$V_B(dC_B/dt) = Q_{LU}(C_{LU}/K_{p,LU} - C_B) - CL_RC_B$$

Lung:

$$V_{LU}(dC_{LU}/dt) = Q_{BR}C_{BR}/K_{p,BR} + Q_{MU}C_{MU}/K_{p,MU} + Q_RC_R/K_{p,R} + Q_HC_{HE5} - Q_{LU}C_{LU}/K_{p,LU}$$

Brain, muscle, kidney:

$$V_i(dC_i/dt) = Q_i(C_B - C_i/K_{p,i})$$

Liver 1 to 5:

(1) rat $(V_{Hi}/5)(dC_{Hi}/dt) = (V_{m,inf}/5)f_BC_{HEi}/(K_{m,inf} + f_BC_{HEi}) + (PS_{dif}/5)f_BC_{HEi} - (PS_{dif}/5)f_TC_{Hi} - (V_{m,bile}/5)f_TC_{Hi}/(K_{m,bile} + f_TC_{Hi}) - (V_{m,met}/5)f_TC_{Hi}/(K_{m,met} + f_TC_{Hi})$

(2) human $(V_{Hi}/5)(dC_{Hi}/dt) = (PS_{inf}/5)f_BC_{HEi} + (PS_{dif}/5)f_BC_{HEi} - (PS_{dif}/5)f_TC_{Hi} - (PS_{bile}/5)f_TC_{Hi} - (CL_{met}/5)f_TC_{Hi}$

Liver extracellular compartment 1:

(1) rat $(V_{HE1}/5)(dC_{HE1}/dt) = Q_H(C_B - C_{HEi}) - (V_{m,inf}/5)f_BC_{HEi}/(K_{m,inf} + f_BC_{HEi}) - (PS_{dif}/5)f_BC_{HEi} + (PS_{dif}/5)f_TC_{Hi}$

(2) human $(V_{HE1}/5)(dC_{HE1}/dt) = Q_H(C_B - C_{HEi}) - (PS_{inf}/5)f_BC_{HEi} - (PS_{dif}/5)f_BC_{HEi} + (PS_{dif}/5)f_TC_{Hi} + k_aF_aX_{GI}$

Liver extracellular compartments 2 to 5:

(1) rat $(V_{HEi}/5)(dC_{HEi}/dt) = Q_H(C_{HE(i-1)} - C_{HEi}) - (V_{m,inf}/5)f_BC_{HEi}/(K_{m,inf} + f_BC_{HEi}) - (PS_{dif}/5)f_BC_{HEi} + (PS_{dif}/5)f_TC_{Hi}$

(2) human $(V_{HEi}/5)(dC_{HEi}/dt) = Q_H(C_{HE(i-1)} - C_{HEi}) - (PS_{inf}/5)f_BC_{HEi} - (PS_{dif}/5)f_BC_{HEi} + (PS_{dif}/5)f_TC_{Hi}$

Bile or gastrointestinal tract:

(1) rat $X_{bile} = \Sigma((V_{m,bile}/5)f_TC_{Hi}/(K_{m,bile} + f_TC_{Hi}))$

(2) human $X_{GI} = \Sigma(PS_{bile}/5)f_TC_{Hi} - (k_aFa)X_{GI}$

Appendix II: Effect of Renal Clearance on the Impact of the Change in the Uptake Clearance on the AUC of the Plasma and Liver

Q_h and CL_r represent the hepatic blood flow and renal clearance, respectively. PS_{inf}, PS_{eff}, and CL_{int} are hepatic uptake, sinusoidal efflux, and intrinsic sequestration clearances, respectively. V and C represent volume and concentration, respectively. Subscripts b, i, and h represent blood, inlet, and liver, respectively. Mass balance differential equations for each compartment in the simple model shown in Fig. 8 are as follows:

$$V_b \cdot \frac{dC_b}{dt} = Q_h(C_i - C_b) - CL_r \cdot C_b$$

$$V_i \cdot \frac{dC_i}{dt} = Q_h(C_b - C_i) - f_b \cdot PS_{inf} \cdot C_i + f_h \cdot PS_{eff} \cdot C_h$$

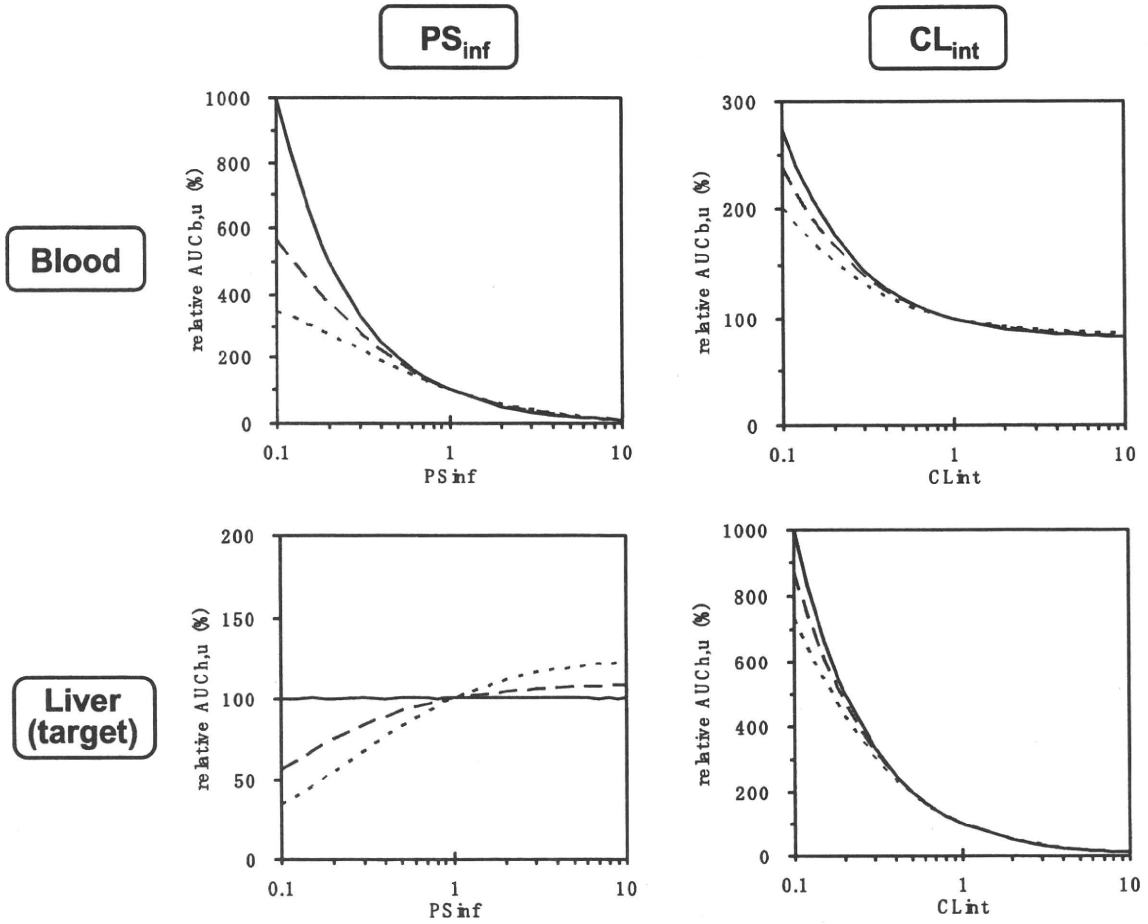

Fig. 9. Effects of renal clearance on the impact of changes in hepatic uptake and intrinsic sequestration clearances on the AUC of pravastatin in the blood and liver. Relative AUC (100% as the initial value) were estimated by varying the uptake and intrinsic sequestration clearances over a 0.1- to 10-fold range of the initial value when the renal clearance was 0 (——), 4 (– – –), and 16 (· · · · · ·) ml/min/kg.

$$V_h \cdot \frac{dC_h}{dt} = f_b \cdot PS_{inf} \cdot C_i - f_h \cdot (PS_{eff} + CL_{int}) \cdot C_h$$

Integrating these equations gives:

$$\frac{\text{Dose}}{f_b \cdot AUC_b} = \frac{PS_{inf} \cdot CL_{int}}{PS_{eff} + CL_{int}} \cdot \frac{CL_r + Q_h}{Q_h} + \frac{CL_r}{f_b} \quad \text{(A1)}$$

$$\frac{\text{Dose}}{f_h \cdot AUC_h} = CL_{int} + \frac{Q_h \cdot CL_r}{CL_r + Q_h} \cdot \frac{PS_{eff} + CL_{int}}{f_b \cdot PS_{inf}} \quad \text{(A2)}$$

where AUC_b and AUC_h represent the area under the concentration-time curve for the blood and liver, respectively. Substituting $CL_R = 0$ yields:

$$\frac{\text{Dose}}{f_b \cdot AUC_b} = PS_{inf} \cdot \frac{CL_{int}}{PS_{eff} + CL_{int}} \quad \text{(A3)}$$

$$\frac{\text{Dose}}{f_h \cdot AUC_h} = CL_{int} \quad \text{(A4)}$$

Equations A3 and A4 indicate that AUC_h depends only on CL_{int} when the renal clearance is negligible. In contrast, AUC_b is inversely proportional to PS_{inf}. If the renal clearance is maximal, that is, the renal blood flow (Q_r), eq. A2 can be converted to:

$$\frac{\text{Dose}}{f_h \cdot AUC_h} = CL_{int} + Q \cdot \frac{PS_{eff} + CL_{int}}{f_b \cdot PS_{inf}} \quad \text{(A5)}$$

where

$$Q = \frac{Q_h \cdot Q_r}{Q_r + Q_h} \approx 9$$

When the hepatic uptake is the rate-limiting process, so $CL_{int} \gg PS_{eff}$, eq. A5 can be converted to:

$$R = \frac{\text{Dose}}{f_h \cdot AUC_h} = CL_{int}\left(1 + Q \cdot \frac{CL_{int}}{f_b \cdot PS_{inf}}\right) \quad \text{(A6)}$$

In accordance, the R value can be higher than CL_{int} by up to $Q \times CL_{int}/(f_b \times PS_{inf})$. Figure 9 shows the effects of renal clearance on the impact of the changes in hepatic uptake and intrinsic sequestration clearance on the AUC of pravastatin in the plasma and liver. A simulation was performed using eqs. A1 and A2 and the parameters shown in Tables 1 and 2,

when the renal clearance was 0, 4 (one quarter of the renal blood flow), and 16 (the renal blood flow) ml/min/kg b.wt.

Acknowledgments

We thank Ayako Takada and Yuji Sekiya for excellent technical assistance.

References

Davies B and Morris T (1993) Physiological parameters in laboratory animals and humans. *Pharm Res* **10**:1093–1095.

Ghibellini G, Vasist LS, Leslie EM, Heizer WD, Kowalsky RJ, Calvo BF, and Brouwer KL (2007) In vitro-in vivo correlation of hepatobiliary drug clearance in humans. *Clin Pharmacol Ther* **81**:406–413.

Giacomini KM and Sugiyama Y (2005) Membrane transporters and drug response, in *Goodman & Gilman's The Pharmacological Basis of Therapeutics* (Brunton LL, Lazo JS, and Parker KL eds), 11th ed, pp 41–70, McGraw-Hill, New York.

Hasegawa M, Kusuhara H, Sugiyama D, Ito K, Ueda S, Endou H, and Sugiyama Y (2002) Functional involvement of rat organic anion transporter 3 (rOat3; Slc22a8) in the renal uptake of organic anions. *J Pharmacol Exp Ther* **300**:746–753.

Ishigami M, Tokui T, Komai T, Tsukahara K, Yamazaki M, and Sugiyama Y (1995) Evaluation of the uptake of pravastatin by perfused rat liver and primary cultured rat hepatocytes. *Pharm Res* **12**:1741–1745.

Iwatsubo T, Hirota N, Ooie T, Suzuki H, Shimada N, Chiba K, Ishizaki T, Green CE, Tyson CA, and Sugiyama Y (1997) Prediction of in vivo drug metabolism in the human liver from in vitro metabolism data. *Pharmacol Ther* **73**:147–171.

Jones HM, Parrott N, Jorga K, and Lavé T (2006) A novel strategy for physiologically based predictions of human pharmacokinetics. *Clin Pharmacokinet* **45**:511–542.

Kawai R, Lemaire M, Steimer JL, Bruelisauer A, Niederberger W, and Rowland M (1994) Physiologically based pharmacokinetic study on a cyclosporin derivative, SDZ IMM 125. *J Pharmacokinet Biopharm* **22**:327–365.

Kawai R, Mathew D, Tanaka C, and Rowland M (1998) Physiologically based pharmacokinetics of cyclosporine A: extension to tissue distribution kinetics in rats and scale-up to human. *J Pharmacol Exp Ther* **287**:457–468.

Kitazawa E, Tamura N, Iwabuchi H, Uchiyama M, Muramatsu S, Takahagi H, and Tanaka M (1993) Biotransformation of pravastatin sodium: I. Mechanisms of enzymic transformation and epimerization of an allylic hydroxy group of pravastatin sodium. *Biochem Biophys Res Commun* **192**:597–602.

Kivistö KT and Niemi M (2007) Influence of drug transporter polymorphisms on pravastatin pharmacokinetics in humans. *Pharm Res* **24**:239–247.

Komai T, Kawai K, Tokui T, Tokui Y, Kuroiwa C, Shigehara E, and Tanaka M (1992) Disposition and metabolism of pravastatin sodium in rats, dogs and monkeys. *Eur J Drug Metab Pharmacokinet* **17**:103–113.

Lennernäs H and Fager G (1997) Pharmacodynamics and pharmacokinetics of the HMG-CoA reductase inhibitors: similarities and differences. *Clin Pharmacokinet* **32**:403–425.

Link E, Parish S, Armitage J, Bowman L, Heath S, Matsuda F, Gut I, Lathrop M, and Collins R (2008) SLCO1B1 variants and statin-induced myopathy: a genome-wide study. *N Engl J Med* **359**:789–799.

Maeda K, Ieiri I, Yasuda K, Fujino A, Fujiwara H, Otsubo K, Hirano M, Watanabe T, Kitamura Y, Kusuhara H, et al. (2006) Effects of organic anion transporting polypeptide 1B1 haplotype on pharmacokinetics of pravastatin, valsartan, and temocapril. *Clin Pharmacol Ther* **79**:427–439.

Miyauchi S, Sawada Y, Iga T, Hanano M, and Sugiyama Y (1993) Comparison of the hepatic uptake clearances of fifteen drugs with a wide range of membrane permeabilities in isolated rat hepatocytes and perfused rat livers. *Pharm Res* **10**:434–440.

Morimoto K, Oishi T, Ueda S, Ueda M, Hosokawa M, and Chiba K (2004) A novel variant allele of OATP-C (SLCO1B1) found in a Japanese patient with pravastatin-induced myopathy. *Drug Metab Pharmacokinet* **19**:453–455.

Nakagomi-Hagihara R, Nakai D, and Tokui T (2007) Inhibition of human organic anion transporter 3 mediated pravastatin transport by gemfibrozil and the metabolites in humans. *Xenobiotica* **37**:416–426.

Nakai D, Nakagomi R, Furuta Y, Tokui T, Abe T, Ikeda T, and Nishimura K (2001) Human liver-specific organic anion transporter, LST-1, mediates uptake of pravastatin by human hepatocytes. *J Pharmacol Exp Ther* **297**:861–867.

Naritomi Y, Terashita S, Kimura S, Suzuki A, Kagayama A, and Sugiyama Y (2001) Prediction of human hepatic clearance from in vivo animal experiments and in vitro metabolic studies with liver microsomes from animals and humans. *Drug Metab Dispos* **29**:1316–1324.

Niemi M, Pasanen MK, and Neuvonen PJ (2006) SLCO1B1 polymorphism and sex affect the pharmacokinetics of pravastatin but not fluvastatin. *Clin Pharmacol Ther* **80**:356–366.

Niinuma K, Kato Y, Suzuki H, Tyson CA, Weizer V, Dabbs JE, Froehlich R, Green CE, and Sugiyama Y (1999) Primary active transport of organic anions on bile canalicular membrane in humans. *Am J Physiol* **276**:G1153–G1164.

Nishizato Y, Ieiri I, Suzuki H, Kimura M, Kawabata K, Hirota T, Takane H, Irie S, Kusuhara H, Urasaki Y, et al. (2003) Polymorphisms of OATP-C (SLC21A6) and OAT3 (SLC22A8) genes: consequences for pravastatin pharmacokinetics. *Clin Pharmacol Ther* **73**:554–565.

Obach RS (1999) Prediction of human clearance of twenty-nine drugs from hepatic microsomal intrinsic clearance data: an examination of in vitro half-life approach and nonspecific binding to microsomes. *Drug Metab Dispos* **27**:1350–1359.

Rane A, Wilkinson GR, and Shand DG (1977) Prediction of hepatic extraction ratio from in vitro measurement of intrinsic clearance. *J Pharmacol Exp Ther* **200**:420–424.

Roberts MS and Rowland M (1986) Correlation between in-vitro microsomal enzyme activity and whole organ hepatic elimination kinetics: analysis with a dispersion model. *J Pharm Pharmacol* **38**:177–181.

Sawada Y, Hanano M, Sugiyama Y, and Iga T (1985) Prediction of the disposition of nine weakly acidic and six weakly basic drugs in humans from pharmacokinetic parameters in rats. *J Pharmacokinet Biopharm* **13**:477–492.

Shitara Y, Horie T, and Sugiyama Y (2006a) Transporters as a determinant of drug clearance and tissue distribution. *Eur J Pharm Sci* **27**:425–446.

Shitara Y, Itoh T, Sato H, Li AP, and Sugiyama Y (2003) Inhibition of transporter-mediated hepatic uptake as a mechanism for drug-drug interaction between cerivastatin and cyclosporin A. *J Pharmacol Exp Ther* **304**:610–616.

Shitara Y and Sugiyama Y (2006b) Pharmacokinetic and pharmacodynamic alterations of 3-hydroxy-3-methylglutaryl coenzyme A (HMG-CoA) reductase inhibitors: drug-drug interactions and interindividual differences in transporter and metabolic enzyme functions. *Pharmacol Ther* **112**:71–105.

Singhvi SM, Pan HY, Morrison RA, and Willard DA (1990) Disposition of pravastatin sodium, a tissue-selective HMG-CoA reductase inhibitor, in healthy subjects. *Br J Clin Pharmacol* **29**:239–243.

Soars MG, Grime K, Sproston JL, Webborn PJ, and Riley RJ (2007) Use of hepatocytes to assess the contribution of hepatic uptake to clearance in vivo. *Drug Metab Dispos* **35**:859–865.

Takane H, Miyata M, Burioka N, Shigemasa C, Shimizu E, Otsubo K, and Ieiri I (2006) Pharmacogenetic determinants of variability in lipid-lowering response to pravastatin therapy. *J Hum Genet* **51**:822–826.

Yamaoka K, Tanigawara Y, Nakagawa T, and Uno T (1981) A pharmacokinetic analysis program (multi) for microcomputer. *J Pharmacobiodyn* **4**:879–885.

Yamazaki M, Akiyama S, Ni'inuma K, Nishigaki R, and Sugiyama Y (1997) Biliary excretion of pravastatin in rats: contribution of the excretion pathway mediated by canalicular multispecific organic anion transporter. *Drug Metab Dispos* **25**:1123–1129.

Yamazaki M, Akiyama S, Nishigaki R, and Sugiyama Y (1996a) Uptake is the rate-limiting step in the overall hepatic elimination of pravastatin at steady-state in rats. *Pharm Res* **13**:1559–1564.

Yamazaki M, Kobayashi K, and Sugiyama Y (1996b) Primary active transport of pravastatin across the liver canalicular membrane in normal and mutant Eisai hyperbilirubinemic rats. *Biopharm Drug Dispos* **17**:607–621.

Yamazaki M, Suzuki H, Hanano M, Tokui T, Komai T, and Sugiyama Y (1993) $Na^{(+)}$-independent multispecific anion transporter mediates active transport of pravastatin into rat liver. *Am J Physiol* **264**:G36–G44.

Yamazaki M, Tokui T, Ishigami M, and Sugiyama Y (1996c) Tissue-selective uptake of pravastatin in rats: contribution of a specific carrier-mediated uptake system. *Biopharm Drug Dispos* **17**:775–789.

Zhang W, Chen BL, Ozdemir V, He YJ, Zhou G, Peng DD, Deng S, Xie QY, Xie W, Xu LY, et al. (2007) SLCO1B1 521T→C functional genetic polymorphism and lipid-lowering efficacy of multiple-dose pravastatin in Chinese coronary heart disease patients. *Br J Clin Pharmacol* **64**:346–352.

Address correspondence to: Dr. Yuichi Sugiyama, Department of Molecular Pharmacokinetics, Graduate School of Pharmaceutical Sciences, University of Tokyo, 7-3-1 Hongo, Bunkyoku-Tokyo 113-0033, Japan. E-mail: sugiyama@mol.f.u-tokyo.ac.jp

Archives of Biochemistry and Biophysics xxx (2008) xxx–xxx

Contents lists available at ScienceDirect

Archives of Biochemistry and Biophysics

journal homepage: www.elsevier.com/locate/yabbi

Thyroid hormone receptor mediates human *MDR1* gene expression—Identification of the response region essential for gene expression

Kouichi Kurose *, Mayumi Saeki, Masahiro Tohkin, Ryuichi Hasegawa

Division of Medicinal Safety Science, National Institute of Health Sciences, 1-18-1 Kamiyoga, Setagaya-ku, Tokyo 158-8501, Japan

ARTICLE INFO

Article history:
Received 30 December 2007
and in revised form 18 March 2008
Available online xxxx

Keywords:
P-glycoprotein (P-gp)
TR
Triiodothyronine (T3)
Thyroxine (T4)
Thyroid hormone response element (TRE)
ABCB1

ABSTRACT

P-glycoprotein, encoded by the *MDR1* gene, is a drug efflux transporter that is expressed in various tissues and plays an important role in the absorption and elimination of many drugs and xenobiotics. Induction of the *MDR1* gene affects drug disposition and the efficacy of drug treatment. In this study, we demonstrated that the thyroid hormone receptor (TR) induces *MDR1* gene expression in a thyroid hormone (TH)-dependent manner. The 5′-upstream region of the human *MDR1* gene was examined for the presence of TH-responsive elements. Luciferase-reporter gene assays revealed that the TH response region is located between −7.9 and −7.8 kb upstream from the transcription start site of *MDR1*. The region contains two TH response clusters, one of which includes a direct repeat with a three-nucleotide spacer (DR3) and a four-nucleotide spacer DR4(I), and the other of which includes two DR4s (II and III). Mutation analyses indicated that every direct repeat has a unique contribution to the TH response. In particular, DR4(I) was shown to be the most important element. Chromatin immunoprecipitation assays revealed that TR and retinoid X receptor (RXR) bind to the TH response region, and gel mobility shift assays confirmed that one molecule of TR/RXR heterodimer binds to each of the clusters in this region, with preferential binding to the upstream one. We furthermore demonstrated that two molecules of TR/RXR could bind simultaneously to the TH response region. The order of binding affinity to the direct repeats was DR4(I) > DR4(II) > DR4(III) ≈ DR3. Our results indicate that these two closely spaced TR/RXR-binding clusters are both required for the maximal induction of *MDR1* gene expression mediated by TR.

The *MDR1* (*ABCB1*) gene plays an important role in pharmacokinetics through the expression of efflux pump P-glycoprotein (P-gp)[1], which has a broad substrate specificity and tissue-specific distribution. P-gp is expressed at high levels on the apical/luminal surface of barrier (blood–brain barrier, intestine, placenta, blood–testis, and blood–ovarian barriers) and excretory (liver, kidney, adrenal gland) tissues, suggesting that P-gp can limit the cellular uptake of drugs into the brain, testis, fetus, and enterocytes and can eliminate drugs into the bile, urine, and intestinal lumen [1,2]. The expression of *MDR1* is induced by a variety of drugs, affecting pharmacokinetics and leading to a decrease in the systemic exposure of drugs that serve as P-gp substrates. The inducers, inhibitors, and tissue distribution patterns of P-gp and CYP3A4 overlap extensively, with the latter being the most abundantly expressed human cytochrome P450 that contributes to the metabolism of a wide spectrum of pharmaceutical drugs and xenobiotics [3,4]. Consequently, the expressions of *MDR1* and *CYP3A4* were expected to have similar induction mechanisms. In fact, the induction of both *MDR1* and *CYP3A4* was found to be mediated through transcriptional activation by the binding of nuclear receptors, such as pregnane X receptor (PXR) and constitutive androstane receptor (CAR), to distal enhancer elements located approximately 8 kb upstream from the transcription start sites of *MDR1* and *CYP3A4* [5–8].

In vivo drug transport can be radically changed by a variety of pathophysiological states, including thyroid dysfunction. For example, in patients with hyperthyroidism who are receiving digoxin—a well-known P-gp substrate—the renal clearance of digoxin is higher and the plasma concentration of digoxin is lower than after normalization of thyroid function [9]. P-gp expressed in the kidneys and intestine has a substantial effect on the urinary and plasma concentration of orally administered P-gp substrates. For example, the intestinal P-gp content is correlated with the AUC after the oral administration of digoxin [10]. Therefore, the alterations in the pharmacokinetics of digoxin in patients with hyperthyroidism can be explained by the induction of P-gp; in other words, the expression level of *MDR1* may increase in patients with hyperthyroidism which is characterized by higher levels of thyroid hormone. Siegmund et al. reported that the expression of intestinal

* Corresponding author. Fax: +81 3 3700 9788.
E-mail address: kurose@nihs.go.jp (K. Kurose).

[1] *Abbreviations used:* P-gp, P-glycoprotein; TH, thyroid hormone; TR, thyroid hormone receptor; DR, direct repeat; PXR, pregnane X receptor; CAR, constitutive androstane receptor; RXR, retinoid X receptor; TRE, thyroid hormone response element; UpC, upstream cluster; DwC, downstream cluster; CYP, cytochrome P450; MDR1, multidrug resistance 1; FITC, fluorescein isothiocyanate; ChIP, chromatin immunoprecipitation.

0003-9861/$ - see front matter © 2008 Elsevier Inc. All rights reserved.
doi:10.1016/j.abb.2008.03.020

Please cite this article in press as: K. Kurose et al., Arch. Biochem. Biophys. (2008), doi:10.1016/j.abb.2008.03.020

P-gp increased after the oral administration of thyroxine (T4) in duodenal biopsy samples obtained from healthy human volunteers [11]. Mitin et al. demonstrated that T4 induced MDR1 mRNA and P-gp in human colon carcinoma cell lines [12]. Although these results indicate that thyroid hormone (TH) is involved in the induction of *MDR1* gene expression, there have been no direct evidence that the thyroid hormone receptor (TR) is involved in the induction.

THs, 3,5,3′-triiodothyronine (T3) and T4, modulate gene expression by interacting with thyroid hormone receptors (TRs), α and β, which are members of the nuclear receptor superfamily [13]. T3 is the principal active and main ligand of TR and is derived by the deiodination of T4. TRα and TRβ, encoded by two distinct genes—*THRA* (*NR1A1*) and *THRB* (*NR1A2*) [13,14], bind T3 and, with a lesser affinity, T4, and mediate TH-regulated gene expression. TR binds to TH-responsive element (TRE), typically as a heterodimer with retinoid X receptor (RXR). TREs consist of a direct repeat, an everted repeat, or an inverted repeat of the consensus hexamer (half-site) sequence of (G/A)GGT(C/G)A separated by a spacer that is several nucleotides long; in particular, DR4 (a direct repeat separated by four nucleotides) is a preferential site for TR binding [15].

Overt thyroid dysfunction is common in the general population [16]. Hypothyroidism is a common disorder affecting many people, especially those over the age of 60 years [17,18]. Patients with hypothyroidism are usually treated with TH replacement therapy. Since TH is widely prescribed and influences the induction of P-gp, which potentially affects pharmacokinetics, the role of TH in the mechanism of *MDR1* expression may be a worthwhile topic of study. In this study, we investigated the molecular mechanism of *MDR1* induction by TH using intestinal epithelial cell lines. We demonstrated that TR/RXR heterodimers bind to the TREs located −7.9 to −7.8 kb upstream from the transcription start site of *MDR1*, which is essential for the induction of *MDR1* by TH.

Materials and methods

Cell cultures and hormone treatment

Human intestinal epithelial cell lines LS180 and Caco-2 were obtained from American Type Culture Collection (Manassas, VA) and were routinely cultured in DME low-glucose medium D6046 (Sigma) containing 10% heat-inactivated fetal bovine serum (FBS), 1× nonessential amino acids (Life Technology), and penicillin (100 IU/ml)/streptomycin (100 μg/ml) (Life Technology) at 37 °C in a humidified atmosphere of 5% CO_2. To study the thyroid hormone actions, the medium was substituted with phenol red-free DME medium (Gibco, Invitrogen) supplemented with 10% dextran-coated charcoal-treated fetal bovine serum (Hyclone Inc.) for 24 h prior to treatment with vehicle (2 mM NaOH), L-thyroxine (T4, Sigma), 3,3′,5,-triiodo-L-thyronine (T3, Sigma), or 3,3′,5′,-triiodo-L-thyronine (rT3, Sigma). T4, T3, and rT3 stock solutions were prepared in 0.2 M NaOH and were added to the medium at a final concentration of 2 mM NaOH. For the time course experiments, LS180 cells were treated with T4 (5 μM) for 4–24 h followed by RNA preparation. For the concentration–response studies, LS180 cells were exposed to 0–1 μM T4, 0–25 nM T3, or 0–25 nM rT3 for 15 h followed by RNA preparation.

Quantitative reverse transcription-polymerase chain reaction (qRT-PCR)

At the end of the TH treatments, RNA and cDNA were prepared from cells using the Fastlane Cell cDNA Kit (Qiagen), following the manufacturer's instructions. The relative expression levels of MDR1, CYP3A4, and UGT1A1 mRNAs were measured using quantitative real-time PCR and the comparative C_t method, described by Applied Biosystems. The relative level of β-actin was also measured as an endogenous reference. The primers and probes for the MDR1, CYP3A4, and UGT1A1 cDNAs were all TaqMan Gene Expression Assays or Assays-on-Demand products from Applied Biosystems. For the normalization of the expression data, the Pre-Developed TaqMan Assay Reagents Endogenous Control human β-actin Kit (VIC-labeled probe; Applied Biosystems) was used. Real-time PCR was performed in 25-μl reactions using the Prism 7000 Sequence Detection System (Applied Biosystems), and the data were analyzed according to the manufacturer's guidelines. Each value represents the mean ± SD of four independent experiments. The fold induction was calculated relative to the untreated cells for each gene.

Plasmids

The *MDR1* 5′-flanking region (−10082/+117) was amplified using the TaKaLa LA PCR Kit (Takara) and genomic DNA prepared from LS180 cells as a template and the primer pairs 5′-CTGGTACCTTGTCATTGTTGAGAAGACGCTG-3′ and 5′-ACGCGTCGACG AACGGCCACCAAGACGTGAA-3′, which include the Kpn I and Sal I sites for cloning. The amplified fragment was digested by Kpn I and Sal I enzymes and ligated to the Kpn I/Xho I site of firefly luciferase rapid response reporter vector pGL4.12 (Promega), resulting in pMD10082L. The plasmids pMD7970L, pMD7145L, and pMD457L were constructed by deleting the Nhe I, Nhe I/Xcm I, and Sph I fragments from pMD10082L, respectively. pMD*824L was constructed by deleting the Xcm I/Sph I fragment from pMD7970L. pMD*824Δ90L, pMD*824Δ153L, and pMD*824Δ214L were constructed using pMD*824L as a template and the In-Fusion Dry-Down PCR Cloning Kit (Clontech) with a reverse common primer 5′-TCTG CAGTGGTCTTTCTTCAG-3′ and forward individual primers 5′-AAAAGGGGATGCTAG ACGTTACCTCATTGAACTAACTTGA-3′, 5′-AAAAGGGGATGCTAGGTTCAAAGTCTATGA ATCATAAAACGATAA-3′, and 5′-AAAAGGGGATGCTAGAGCTCTGCAATTCAAAAGCCA-3′, respectively.

Mutations at the half-sites of the direct repeats were introduced into the pMD*824Δ90L reporter plasmid using the Quick-Change Multi Site-Directed Mutagenesis Kit (Stratagene), according to the manufacture's instructions, with the following oligonucleotides used alone or in combination:

M1, 5′-AAGGGGATGCTAGACGTTTTCTCATTGAACTAACTTGAC-3′;
M2, 5′-GCTAGACGTTACCTCATTGTTCTAACTTGACCTTGCTCCTG-3′;
M3, 5′-GAACTAACTTGTTCTTGCTCCTGGG-3′;
M4, 5′-GACCTTGCTCCTGGGAGAGAGAACATTTGAGATTAAACAAG-3′;
M7, 5′-CCTGGGAGAGAGTTCATTTGAGATGGAACAAGTTCAAAGTCTATG-3′; and
M12, 5′-GAGAGAGTTCATTTGAGATTAAACAAGTTTTAAGTCTATGAATC-3′.

All the mutations were verified using DNA sequencing on an Applied Biosystems 3730 sequencer (Applied Biosystems). Human TRβ (TRβ1) cDNA in a pME18SFL3 vector was purchased from Toyobo Co., Ltd. EcoR I and Not I fragments, including the full-length TRβ cDNA, was subcloned into pcDNA3.1 (Invitrogen), resulting in the TRβ expression plasmid pcTRβ. The expression plasmid encoding human RXRα cDNA (pcDNA3.1-hRXRα) was a generous gift from Dr. Shuichi Koizumi (Yamanashi University, Japan).

Transient transfection and luciferase-reporter gene assays

Cells were seeded into 96-well plates and grown until 70–80% confluence, then transiently transfected using HilyMax transcription regent (Dojindo Laboratories, Japan) at a reagent:DNA ratio of 5:1, according to the manufacturer's instructions. One hundred nanograms/well of the luciferase-reporter plasmid to be examined was transfected with 10 ng/well of pcTRβ or pcDNA3.1 and 10 ng/well of pGL4.74 (Promega), a plasmid encoding the *Renilla reniformis* luciferase and used to normalize the transfection efficiency, in 100 μl/well of medium. Twenty-four hours after transfection, the cells were treated with 50 nM of T3. Firefly and *Renilla* luciferase activities were measured 3.5 h after treatment using the Dual-Glo Luciferase kit (Promega) in a Wallac 1420 ARVOsx Multilabel counter (PerkinElmer Life Science). The transfection efficiency of the firefly luciferase activity was normalized against the activity of the internal *Renilla* luciferase activity. The fold induction was calculated as a ratio of (the activity from T3-treated cells)/(the activity from untreated cells). Each value represents the mean ± SD of four independent experiments, in each of which the fold induction value was the ratio of the mean activity from four wells of T3-treated cells divided by the mean activity from four wells of untreated cells.

Chromatin immunoprecipitation (ChIP) assays

Caco-2 cells were transiently transfected with 6 μg/dish (100-mm) of pcTRβ and pcDNA3.1-hRXRα. After incubation for 40 h, the culture medium was changed to phenol red-free DME medium supplemented with 10% dextran-coated charcoal-treated fetal bovine serum. After incubation for 4 h, the cells were used for ChIP assays by using ChIP-IT Express Enzymatic Kit (Active Motif, Inc.) according to the manufacturer's instructions. Immunoprecipitation of the chromatin complexes were performed with an anti-human TRβ1 mouse monoclonal antibody (sc-738; Santa Cruz Biotechnology, Inc.) and anti-human RXRα mouse monoclonal antibody (PP-K8508-00; Perseus Proteomics, Inc.). As a negative control, anti-human PXR mouse monoclonal antibody (PP-H4417-00; Perseus Proteomics, Inc.) was used because PXR is not expressed in the Caco-2 cells. PCR was performed with 5 μl (from a total of 100 μl) of eluted immunoprecipitate or of 1.0% input (chromatin taken before immunoprecipitation) in a total volume of 25 μl for 30 cycles. The set of primers used for the amplification of −7886 to −7730 bp (TR-binding region) were: forward 5′-GAGTGAACGTTACCTCATTGAAC-3′ and reverse 5′-CCGAAATGGCTTTTG AATTG-3′. The set of primers used for the amplification of −9889 to −9762 bp (negative control region) were: forward 5′-AAATATGAGATGCATAGAGCC-3′ and reverse 5′-AACCTTCTTACTCTACTATAGTC-3′. Cycling conditions were 94 °C for 5 min, followed by 30 cycles at 94 °C for 15 s, 55 °C for 30 s, and 72 °C for 15 s. PCR products were resolved on 2.2% FlashGel DNA Cassettes (Lonza Rockland, Inc.).

Please cite this article in press as: K. Kurose et al., Arch. Biochem. Biophys. (2008), doi:10.1016/j.abb.2008.03.020

Gel mobility shift assays

The upper strand sequences of the probes and competitors used in the gel mobility shift assays are shown in Figs. 4 and 5. The double-stranded oligonucleotide corresponding to the −218 to −117 region of the human *PXR* promoter [19] was used as the nonspecific competitor NS. The oligonucleotides that were used as probes and competitors were purchased from Sigma Genosys. Four longer probes of WT, M3, M7, and M21, containing the −7880 to −7788 region of the human *MDR1* gene (Fig. 5), were prepared by PCR amplification using the wild-type (pMD*824Δ90L) and its mutant plasmids (M3, M7, and M21) as templates, respectively, with 5′-fluorescein isothiocyanate (FITC)-labeled primers 5′-AGGGGATGCTAGACGT-3′ and 5′-TTATCGTTTTATGATTCATAGACTT-3′. The DNA fragments were purified using the GFX PCR DNA and Gel Band Purification Kit (GE Healthcare). The TNT T7 Quick Coupled Transcription/Translation System (Promega) was used for *in vitro* synthesis of human TRβ and RXRα proteins from the pcDNA3.1-based full-length cDNA expression plasmids, as recommended by the supplier. DNA–protein complexes were allowed to form by incubating 2.5-μl aliquots of the programmed lysates of TRβ or RXRα alone or mixed at a ratio of 1:1 or unprogrammed reticulocyte lysate with 0.5 μl of 0.33-μM 5′ FITC-labeled double-stranded oligonucleotide probe, 1 μl of 5× binding buffer (87.5 mM KCl, 20 mM $MgCl_2$, 0.5 mM EDTA, 2.5 mM DTT, 2.5 mM PMSF, 50% glycerol and 50 mM HEPES, pH 7.4), and 0.5 μl of 1 mg/ml poly(dI–dC) for 20 min at room temperature (Fig. 4). For the competition assays, the indicated amounts of unlabeled double-stranded competitor oligonucleotides were added simultaneously with the labeled probe. In the assays using the PCR-based probe (Fig. 5), 8 μl of the programmed reticulocyte lysates (TRβ and RXRα at a ratio of 1:2) were incubated with 0.5 μl of FITC-labeled probe, 1 μl of 10× binding buffer (30 mM $MgCl_2$, 1 mM EDTA, 5 mM DTT, 50% glycerol and 200 mM HEPES, pH 7.75), and 0.5 μl of 1 mg/ml poly(dI–dC) for 30 min at room temperature. An aliquot of the reaction mixture was electrophoresed on 4–7% Long Ranger gels (Cambrex) in 0.5× TBE (44.5 mM Tris, 44.5 mM boric acid, and 1.25 mM EDTA) at 500 V at room temperature on a slab gel DNA sequencer DSQ-2000 (Shimadzu).

Results

Thyroid hormone-mediated induction of MDR1

To investigate the induction of *MDR1* by thyroid hormone, an intestinal epithelial cell line, LS180, was used as a model cell line. Although MDR1 mRNA was reported to be induced by T4 (100 nM and 100 μM) after 72 h of exposure in LS180 V and Caco-2 cells [12], we were interested in examining the inducibility of MDR1 mRNA by T3 and T4 more minutely. When LS180 cells were treated with T4, the MDR1 mRNA was induced in a time- and dose-dependent manner (Fig. 1A and B). The relatively rapid induction implies that *MDR1* expression is regulated at the transcriptional level. The induction of *MDR1* was also observed in a T3 dose-dependent manner, but rT3, an inactive metabolite of T3, had no effect on the induction of the MDR1 mRNA (Fig. 1C). These results indicate that the expression of the *MDR1* gene is induced by thyroid hormones (THs) that are known to act through the thyroid hormone receptor (TR).

PXR and CAR, which are members of the nuclear receptor superfamily as well as TR, mediate the gene expression of some drug-metabolizing enzymes and transporters like *CYP3A4*, *UGT1A1*, and also *MDR1*. TR recognizes DNA motifs similar to PXR- or CAR-binding elements. Therefore, it is likely that *CYP3A4* and *UGT1A1* might be induced by TH. Unexpectedly, previous work demonstrated that the expression of *CYP3A4* was not induced by TH [12]. Thus, we examined the inducibility of *UGT1A1* expression by TH in addition to that of *CYP3A4*. As shown in Fig. 1B and C, both T4 and T3 failed to induce the gene expression of *UGT1A1* similar to *CYP3A4*.

Identification of thyroid hormone response region

To investigate the mechanism of *MDR1* gene expression induced by TH, we performed a luciferase-reporter gene assays, using the Caco-2 cell line to exclude the influence of PXR, because Caco-2 is an intestinal epithelial cell line as well as LS180 and expresses TR but not PXR, on the other hand, LS180 expresses both TR and PXR [12,20]. A genomic DNA fragment from −10 kb to +117 bp of the *MDR1* (the major transcription initiation site is designated as

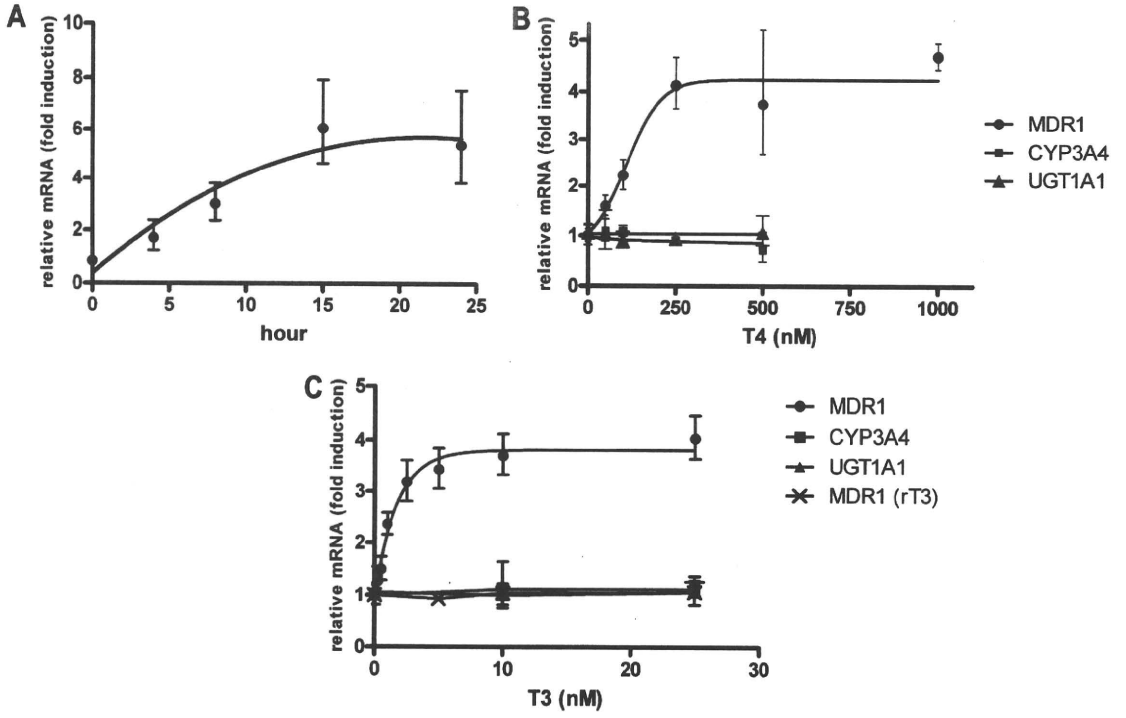

Fig. 1. Thyroid hormone-mediated induction of *MDR1* gene expression in LS180 cells. LS180 cells were treated with thyroid hormones followed by RNA preparation. The mRNA levels were analyzed by qRT-PCR as described in the Materials and methods section. The fold induction was calculated relative to the untreated cells for each gene. Each value represents the mean ± SD of four independent experiments. (A) Time course of T4-mediated induction of *MDR1* gene expression in LS180 cells. LS180 cells were treated with 5 μM T4 for 4, 8, 15, or 24 h followed by RNA preparation. (B) Effect of increasing the dose of T4 on the gene expressions of *MDR1*, *CYP3A4*, and *UGT1A1* in LS180 cells. LS180 cells were treated with 0–1000 nM T4 for 15 h followed by RNA preparation. (C) Effect of increasing the dose of T3 or rT3 on the gene expressions of *MDR1*, *CYP3A4*, and *UGT1A1* in LS180 cells. LS180 cells were treated with 0–25 nM of T3 or rT3 for 15 h followed by RNA preparation.

Please cite this article in press as: K. Kurose et al., Arch. Biochem. Biophys. (2008), doi:10.1016/j.abb.2008.03.020

+1) was subcloned into a luciferase-reporter vector pGL4.12. In the absence of TR expression plasmid pcTRβ, the −10-kb-long construct showed just over a 2-fold induction by T3, as shown in Fig. 2A. By contrast, in the presence of pcTRβ, more than a 10-fold induction was induced by T3. These results indicate that TR mediates the TH response and that the TH response region is located within −10 kb to +117 bp of the *MDR1* gene. Similar results were obtained using LS180 cells (data not shown). To determine the TH response region, we constructed a variety of deletion mutants of *MDR1*-luciferase constructs and carried out a luciferase assay. As shown in Fig. 2A, a 5′-deletion from −7970 to −7145 led to a dramatic loss of inducibility by T3. The lost inducibility was recovered by the deleted region of 824 bp (Fig. 2A, bottom line). To specify the TH response region more precisely, a further 5′-deletion analysis of this 824 bp region was performed. As shown in Fig. 2B, more than a 90-bp deletion (to 153 and 214 bp) from the 5′-end of the 824 bp region caused the almost complete loss of T3 inducibility. Therefore, we concluded that the region between −7880 and −7817 is critical for the T3 response. As shown in Fig. 3A, this critical region includes AGGTCA-like repeats of one DR3 and three DR4(I, II, and III) motifs that are possible nuclear receptor binding sites. To investigate which motifs are responsible for the T3 response, mutant reporter plasmids in which 2-bp mutations were introduced in the half-sites of the direct repeats were constructed and assayed. As shown in Fig. 3A, the possible nuclear receptor response elements are composed of two clusters: the upstream one (UpC) contains DR3 and DR4(I), while the downstream one (DwC) contains DR4(II) and DR4(III). Each cluster also contains three half-sites in which the central half-site is shared by two direct repeats (DRs). Every mutation introduced in each half-site caused the loss of T3 induction to a varying degree (Fig. 3B, M1–M12). Especially, the M3 mutation that is located in the downstream half-site of DR4(I) caused a substantial decrease in inducibility. The double mutation introduced in each cluster (upstream and downstream) led to a much greater reduction than the single mutation (Fig. 3, M19–M23), indicating that every direct repeat makes its own contribution to the T3 response. In particular, DR4(I) seems to be a much more important element.

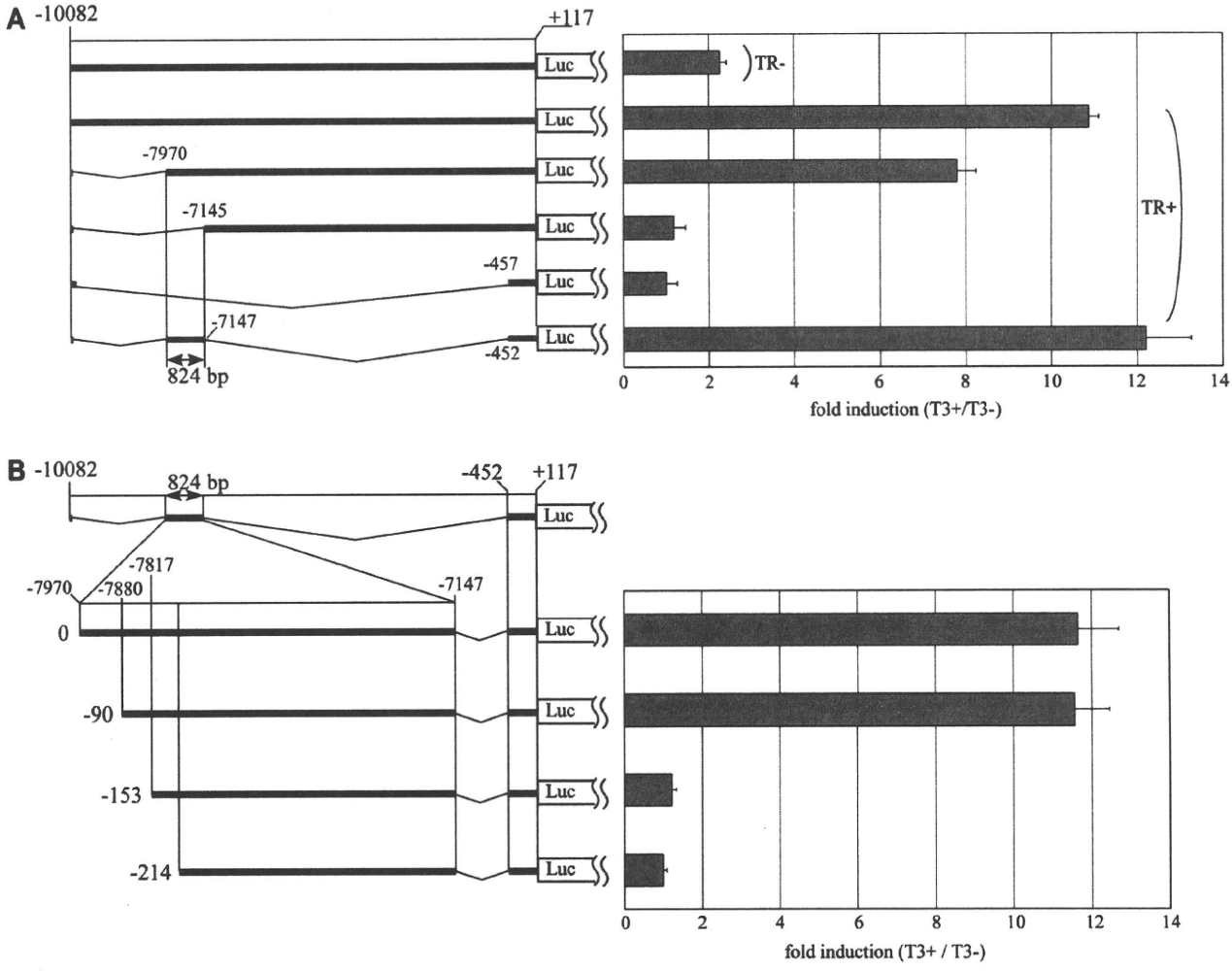

Fig. 2. Transcriptional activity of various *MDR1* 5′-deletion-luciferase-reporter constructs induced by T3 in transiently transfected Caco-2 cells. The luciferase activity was analyzed as described in the Materials and methods section. The fold induction was calculated as a ratio of (the activity from T3-treated cells)/(the activity from untreated cells) and is presented on the right side of each panel. Each value represents the mean ± SD of four independent experiments. The nucleotide positions in relation to the transcription start site are indicated. (A) Schematic presentations of the pMD10082L, pMD7970L, pMD7145L, pMD457L and pMD*824L are shown from the top of the left side. pMD10082L was introduced into the cells with pcDNA3.1 (TR-) or pcTRβ (TR+). The other constructs were introduced into the cells with pcTRβ (TR+). (B) Schematic presentations of pMD*824L, pMD*824Δ90L, pMD*824Δ153L, and pMD*824Δ214L are shown from the top of the left side.

Please cite this article in press as: K. Kurose et al., Arch. Biochem. Biophys. (2008), doi:10.1016/j.abb.2008.03.020

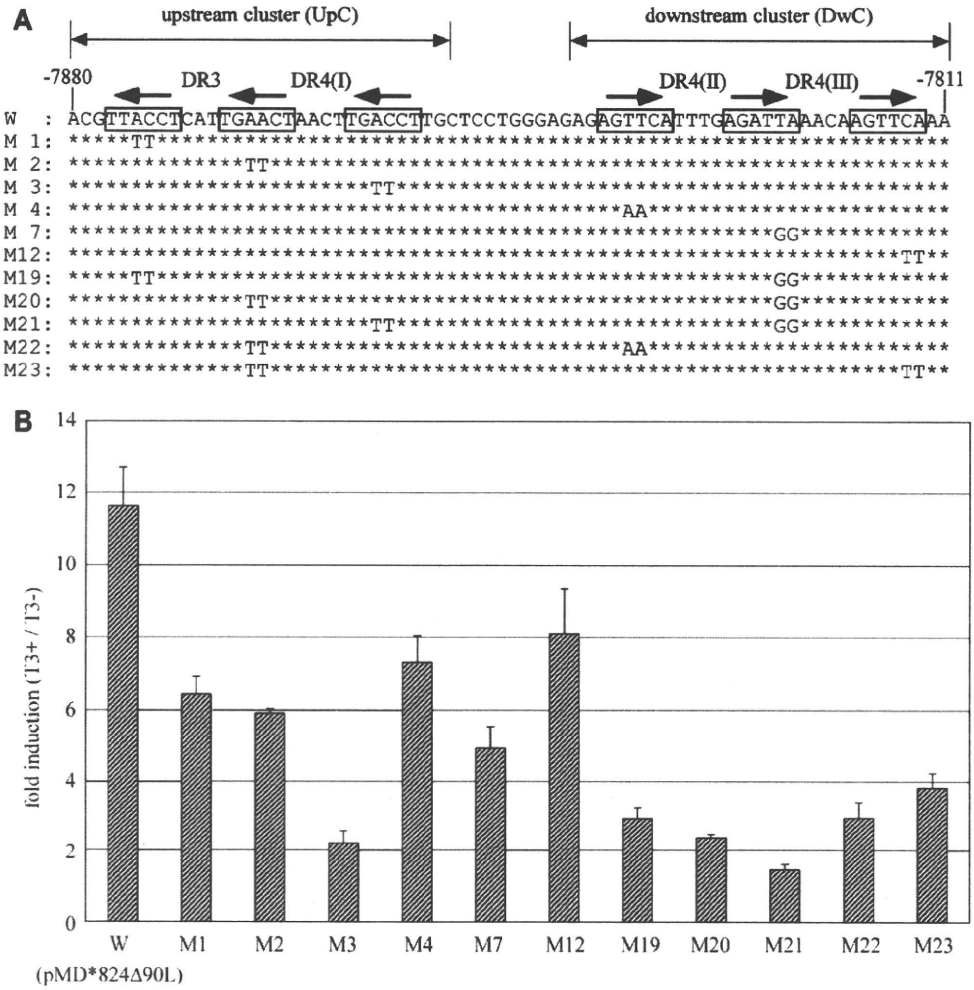

Fig. 3. Influence of different mutations in the thyroid hormone response region located between −7.9 and −7.8 kb upstream of the *MDR1* gene. (A) Based on the reporter plasmid pMD*824Δ90L (designated as W), various mutations were introduced in the half-sites of the direct repeats. The sequences from −7880 to −7811 (relative to the transcription start site of *MDR1*) of the reporter plasmid pMD*824Δ90L and the corresponding mutant plasmids (M1–M23) are indicated. The half-sites of the direct repeats are boxed with arrows that indicate the direction of the direct repeats. Nucleotides identical to the wild-type are shown as asterisks, and mutated nucleotides are shown as letters in the corresponding positions. (B) pMD*824Δ90L and corresponding mutant plasmids were introduced in Caco-2 cells with pcTRβ. The luciferase activity was analyzed as described in the Materials and methods section. The fold induction was calculated as a ratio of (the activity from T3-treated cells)/(the activity from untreated cells). Each value represents the mean ± SD of four independent experiments.

Binding of TR/RXR heterodimer to the thyroid hormone response region

We performed ChIP assays to examine whether TR and RXR are binding to the TH response region using Caco-2 cells transiently transfected with TR and RXR expression plasmids. Immunoprecipitations were performed using antibodies against TR, RXR, or control IgG. As shown in Fig. 4A, antibodies against TR and RXR, but not control IgG, immunoprecipitated the DNA fragments including TH response region. The negative control primers located 2 kb upstream of the TH response region, in which no possible TREs were found, produced no detectable PCR products except from input. These results indicate that TR and RXR are indeed binding to the TH response region in living cells and the TH response region is also TR binding region. We, therefore, hypothesized that the different levels of reduced inducibility in each mutation, as shown in Fig. 3, could be explained by differences in TR binding to the motifs in the thyroid hormone response region. To examine this possibility, we performed gel mobility shift assays using *in vitro* translated TRβ and RXRα to compare the binding affinities of TR/RXR heterodimer with DR3, DR4(I), DR4(II), and DR4(III) in the thyroid hormone response region. The probes and competitors used for the gel-shift assays are summarized in Fig. 4B. As shown in Fig. 4C and D, no protein–DNA complex was observed on any of the DNA motifs when unprogrammed reticulocyte lysates, TR only, or RXR only was used. As shown in Fig. 4C, TR/RXR formed a complex with the UpC probe including DR3 and DR4(I). The complex was eliminated by self-competition but not by nonspecific competition, indicating the sequence-specific binding of TR/RXR to the UpC. Using the DwC, including DR4(II) and DR4(III), as a competitor, the complex was also eliminated (but to a slightly lesser degree). Competitors of M1, M2, and M3 mutant oligonucleotides, including the same mutations as M1, M2, and M3 constructs used in the reporter gene assays in Fig. 3, respectively, inhibited complex formation in the following order: M1 > M2 > M3. In other words, the M3 mutation reduced the ability to form the TR/RXR–DNA complex most strongly. These results agree well with those obtained in the reporter gene assays, in which the M3 mutation strongly reduced transcriptional activation (Fig. 3). Each competitor of the four direct repeats in the thyroid hormone response region

Please cite this article in press as: K. Kurose et al., Arch. Biochem. Biophys. (2008), doi:10.1016/j.abb.2008.03.020

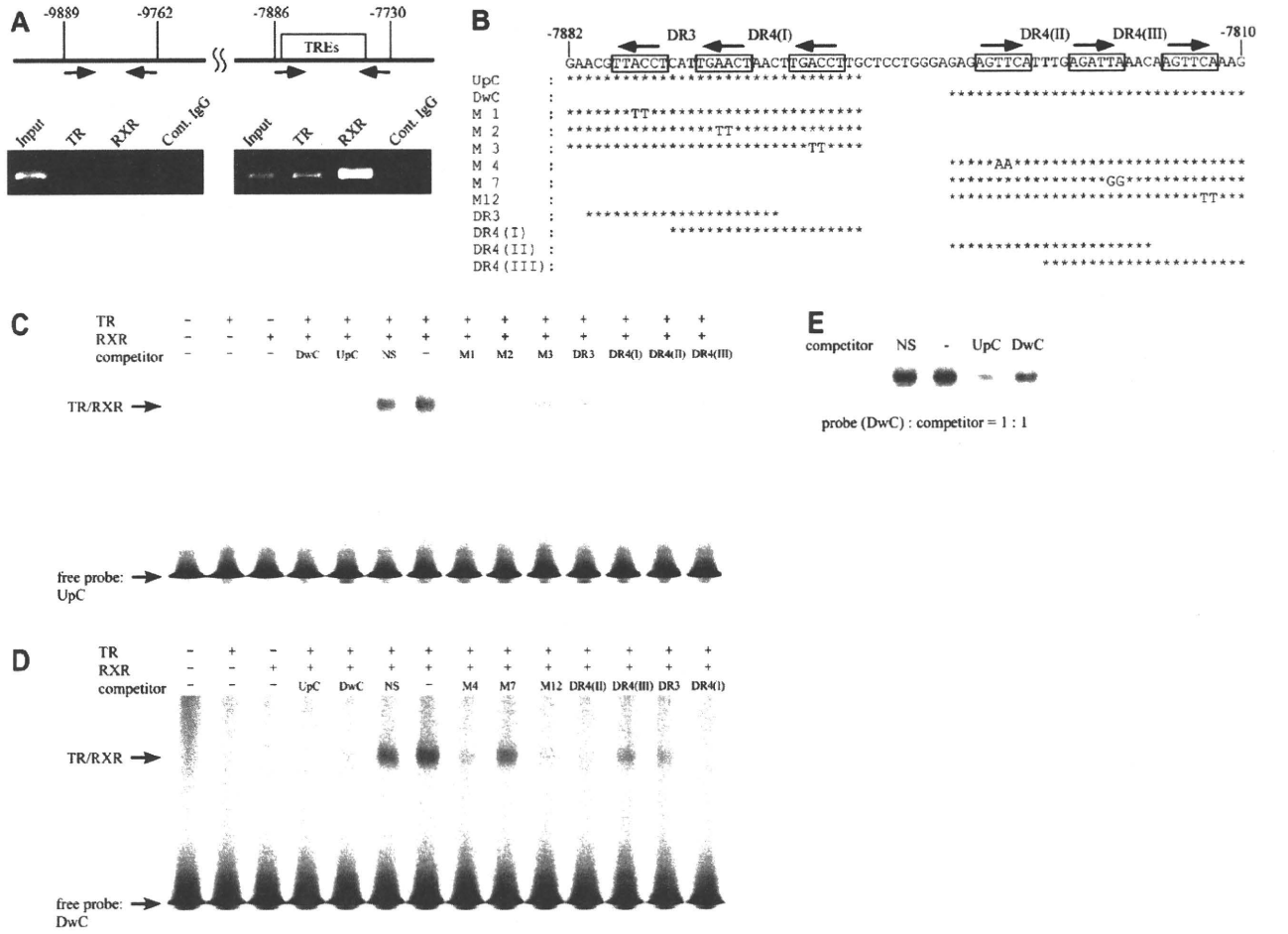

Fig. 4. TR/RXR heterodimer binds to direct repeats in the thyroid hormone response region. (A) TR and RXR binding to the TH response region detected by ChIP assays. The locations of the TH response region (TREs) and primer sets are shown at the top of the figure. Caco-2 cells transiently transfected with TRβ and RXRα expression plasmids were used for ChIP assays. As described in the Materials and methods section, ChIP assays were performed with antibodies against TRβ1, RXR, and control IgG. Input lanes indicate PCR products used soluble chromatin before immunoprecipitation as a template. (B) Oligonucleotide sequences used in the gel mobility shift assays. The nucleotide positions are shown relative to the transcription start site of *MDR1*. The half-sites of the direct repeats are boxed with arrows. Asterisks indicate nucleotides that are the same as the wild-type. (C) Gel mobility shift assay using *in vitro* translated proteins and an FITC-labeled oligonucleotide probe UpC. The labeled UpC probe was incubated with *in vitro* translated TRβ and/or RXRα or with unprogrammed reticulocyte lysate as a control in the presence or absence of a 20-fold molar excess of unlabeled oligonucleotides competitors. The complexes were resolved on a 7% Long Ranger gel. (D) Gel mobility shift assay using *in vitro* translated proteins and an FITC-labeled oligonucleotide probe DwC. The labeled DwC probe was incubated with *in vitro* translated TRβ and/or RXRα, or with unprogrammed reticulocyte lysate as a control in the presence or absence of a 15-fold molar excess of unlabeled oligonucleotides competitors. The complexes were resolved on a 7% Long Ranger gel. (E) Gel mobility shift assay using *in vitro* translated proteins and an FITC-labeled oligonucleotide probe DwC. The labeled DwC was incubated with *in vitro* translated TRβ and RXRα in the presence or absence of equimolar unlabeled oligonucleotide competitors. Complexes were resolved on a 6.5% Long Ranger gel. NS denotes nonspecific competitors, as described in the Materials and methods section.

inhibited the TR/RXR–UpC complex formation in the following order: DR4(I) > DR4(II) > DR3 ≈ DR4(III), as judged by the intensity of the gel-shift bands.

As in the case with the UpC probe, we carried out gel-shift assays with DwC, including DR4(II) and DR4(III), as a probe (Fig. 4D). The sequence-specific binding of TR/RXR to the DwC was confirmed using self- and nonspecific competitors. Mutations introduced into the M4, M7, and M12 competitors, which include the same mutations as the M4, M7, and M12 constructs used in the reporter gene assays, respectively, reduced the binding of TR/RXR, especially M7. These results also agree well with the results obtained in the reporter gene assays shown in Fig. 3. Every direct repeat competitor also competed with the DwC probe in forming a complex with a different affinity. Fig. 4E shows the competitive gel-shift assay with the DwC probe in which equimolar competitors of UpC or DwC were used. The binding affinity of TR/RXR to UpC was confirmed to be larger than that of DwC.

In summary, the TR/RXR heterodimer binds, with different affinity, to two clusters (UpC > DwC) and the DR motifs (DR4(I) > DR4(II) > DR4(III) ≈ DR3).

How many TR/RXR heterodimer molecules bind to the thyroid hormone response region?

We demonstrated that each cluster bound the TR/RXR heterodimer and demonstrated, using competitive gel-shift assays, that each direct repeat alone bound TR/RXR (Fig. 4C and D). Each cluster contains three half-sites in which the central half-site is shared by two direct repeats (Fig. 4B). Therefore, the question that arises is how many molecules of TR/RXR bind to each cluster including the two direct repeats. To examine this, we performed the gel mobility shift assay using the probe of DR4(II) as a representative of a direct repeat that binds one molecule of TR/RXR, in addition to the probes of UpC and DwC

Please cite this article in press as: K. Kurose et al., Arch. Biochem. Biophys. (2008), doi:10.1016/j.abb.2008.03.020

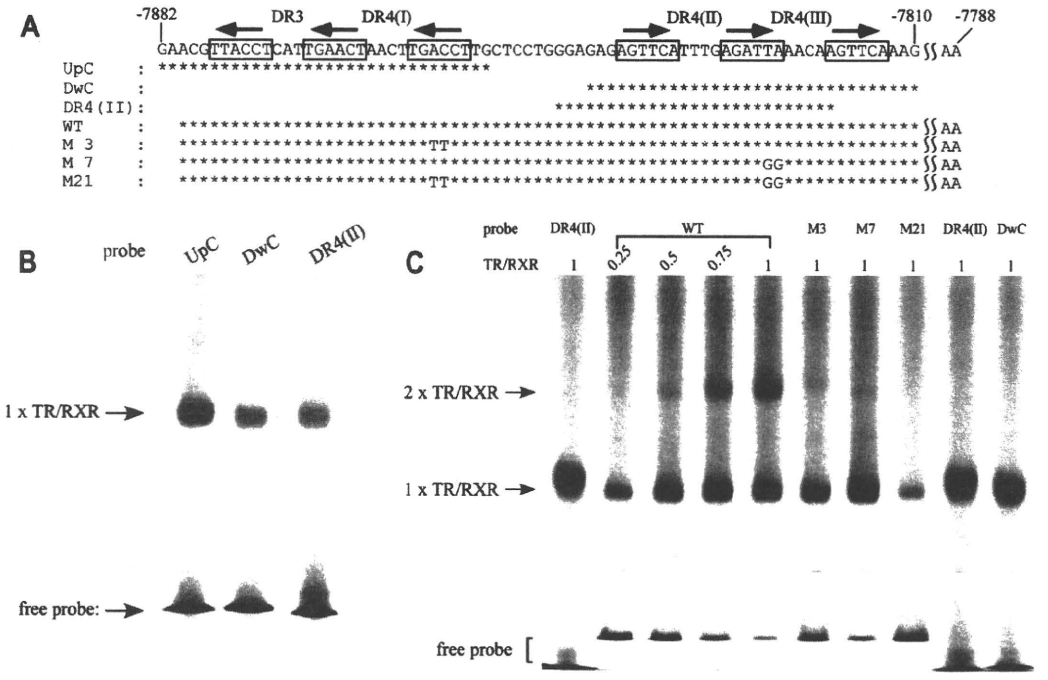

Fig. 5. Two molecules of TR/RXR heterodimer bind to the thyroid hormone response region. (A) Probes used in the gel mobility shift assays. The nucleotide positions are shown relative to the transcription start site of *MDR1*. The half-sites of direct repeats are boxed with arrows. Asterisks indicate nucleotides that are the same as the wild-type. (B) Gel mobility shift assay was performed using *in vitro* translated proteins and FITC-labeled oligonucleotide probes, as indicated. The labeled probes were incubated with *in vitro* translated TRβ and RXRα. The complexes were resolved on a 5% Long Ranger gel. (C) Gel mobility shift assay using *in vitro* translated proteins and the indicated FITC-labeled oligonucleotide probes. The labeled probes were incubated with the indicated amounts of *in vitro* translated TRβ and RXRα. The complexes were resolved on a 4% Long Ranger gel.

(Fig. 5). As shown in Fig. 5B, both UpC- and DwC–TR/RXR complexes exhibited the same mobility as that of the DR4(II)–TR/RXR complex, indicating that one molecule of TR/RXR binds to each cluster. Another question is how many molecules of TR/RXR bind to this region including the two clusters. Each cluster can bind one molecule, suggesting that two molecules of TR/RXR bind to this region, though the two clusters are spaced relatively close. Therefore, longer probes including the two clusters were used as gel-shift probes (Fig. 5A). As shown in Fig. 5C, one shifted band (primary band) was observed when a lower amount of TR/RXR was used with a wild-type longer probe (WT). The mobility of the band was the same as that from the DR4(II) and DwC probes, to which one molecule of TR/RXR binds. Increasing the amount of TR/RXR produced an increasing amount of a slower migrating secondary band that was thought to be a complex containing two molecules of TR/RXR (Fig. 5C). Although the primary bands were generated using M3 and M7 probes, the secondary bands were greatly decreased. Because the M3 and M7 probes contain mutations that reduced the binding of TR/RXR to UpC and DwC, respectively (Fig. 4), a single molecule of TR/RXR should bind to the other non-mutated clusters in both of the probes. Not only the secondary band, but also the primary band nearly disappeared when the M21 probe, which contains both M3 and M7 mutations, was used. These data strongly suggest that two molecules of TR/RXR can bind to this thyroid hormone response region (UpC and DwC) at the same time; at lower concentrations of TR/RXR, however, only one molecule of TR/RXR binds to the region (preferentially to UpC). These results coincide with those in the reporter gene assays, in which each of the M3 and M7 mutations alone could not suppress the transcriptional activation completely, while the M21 mutation abolished the activity (Fig. 3).

Discussion

In previous *in vivo* and *in vitro* studies, the expression of P-gp was induced by T4 [11,12,21,22]. The duodenal expression of P-gp and MDR1 mRNA increased in 8 healthy human volunteers after the oral administration of T4 for 17 days, although the induced level of mRNA was not statistically significant [11]. In rats, the expression levels of P-gp and mdr1a/1b mRNAs increased in a tissue-selective manner after the oral administration of T4 for 3 weeks [21,22]. In intestinal cell lines exposed to T4 for 72 h, MDR1 mRNA expression increased in LS180V cells, while the mRNA and P-gp levels increased in Caco-2 cells [12]. These data were obtained using a relatively long period of T4 exposure. The mechanism responsible for this induction, including whether P-gp was induced by TH directly or indirectly, remained uncertain. In the present study, we demonstrated that the induction of *MDR1* by TH is mediated by TR at the transcriptional level. We showed first the time- and dose-dependent induction of MDR1 mRNA by TH in LS180 cells (Fig. 1). Induction was observed after as few as 4 h, and rT3 had no effect on the induction, implying that the expression of *MDR1* was directly induced by TH through TR. We then conducted luciferase-reporter gene assays (Figs. 2 and 3), ChIP assays (Fig. 4), and gel-shift assays (Figs. 4 and 5), in which we demonstrated that the induction of *MDR1* gene expression by TH is transcriptionally regulated by TR through a TH response region located between −7.9 and −7.8 kb upstream of *MDR1*, including one DR3 and three DR4 motifs (Fig. 6). Previous studies have shown that PXR and CAR, members of the nuclear receptor superfamily as well as TR, mediate the up-regulation of *MDR1* through the response region located −7.9 to −7.8 kb upstream of the *MDR1* using an epithelial cell line LS174T [5,6]. The region responsive for TR was eventually found to be the same as that of PXR and CAR, however, the regulation manners of TR is different

Please cite this article in press as: K. Kurose et al., Arch. Biochem. Biophys. (2008), doi:10.1016/j.abb.2008.03.020

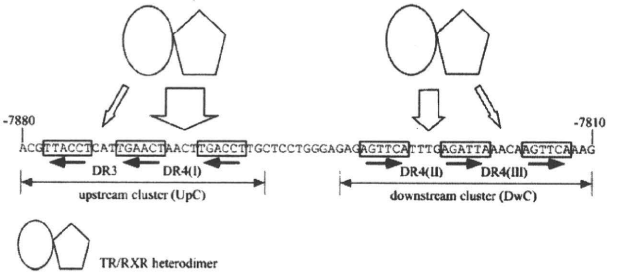

Fig. 6. Two molecules of TR/RXR bind to TH response region located −7.9 to −7.8 kb upstream of the *MDR1* gene with different affinities. The nucleotide positions are shown relative to the transcription start site of *MDR1*. The half-sites of the TREs are boxed. TR/RXR binds to DR3 or DR4(I), and/or DR4(II) or DR4(III) with different affinity, which is denoted by the thickness of the arrow.

from those of PXR and CAR. Geick et al. reported that PXR/RXR bound to three DR4 motifs with the strongest affinity to DR4(III) but did not bind to DR3 [6], whereas TR/RXR bound to all four TREs, including DR3, and bound to DR4(I) preferentially (Fig. 4). The binding affinity was in the following order: DR4(I) > DR4(II) > DR3 ≈ DR4(III) (Fig. 4). As for the transcriptional activity, DR4(I) was the most important element for PXR-mediated induction, similar to TR-mediated induction; however, DR4(III) mutation resulted in an increase in PXR induction [6], which differs from the case of TR. Burk et al. reported that CAR/RXR bound to DR4(I) and to a lesser degree to DR4(III) and that the CAR monomer, but not the CAR/RXR heterodimer, bound to DR4(II) [5]. The transcriptional activity at the region mediated by CAR is similar to that mediated by TR except that the DR4(III) mutation increased the induction by CAR as well as that by PXR. The transcriptional inducibility mediated by TR/RXR coincided with the TR/RXR-binding affinity to the DR motifs (Figs. 3–5). The DR motif with the largest contribution to the transactivation of *MDR1* by TR/RXR was DR4(I), and the other DR motifs likely serve as auxiliary engines for compensation. In recent years, regulatory proteins—including nuclear receptors—have been reported to cross-talk during the regulation of their target genes [23–27]. In this context, we examined the gene expressions of *CYP3A4* and *UGT1A1* by TH in LS180 cells (Fig. 1B and C). In addition to *MDR1* [5,6,28], the gene expressions of both *CYP3A4* and *UGT1A1* are induced by both nuclear receptors PXR and CAR [7,8,29–31], which recognize similar DNA motifs to those of TR. Unexpectedly, both T4 and T3 failed to induce the gene expressions of *CYP3A4* and *UGT1A1*, suggesting that TR is not involved in their gene regulation. Previously, Mitin et al. also reported that *CYP3A4* was not induced by TH. On the basis of the sequence comparison of a DR4 in the −8 kb region of *CYP3A4*, they speculated that the DR4 in *CYP3A4* might be nonfunctional for TR/RXR. Although each of TR, PXR, and CAR has its own manner of regulating *MDR1* expression, their mutual cross-talk may have enhancing or competitive effects on the *MDR1* transcription efficiency, which remains to be elucidated in the future.

Some drugs of P-gp substrates act as P-gp inhibitors that modulate P-gp function by competition for drug-binding sites or by blockading the ATP-hydrolysis process [1,2,32]. Amiodarone, an antiarrhythmic drug and a well-known competitive P-gp inhibitor, has been reported to decrease the activity of type I and type II 5′-deiodinases, which convert T4 to more potent T3 in peripheral tissues. This leads to a reduction in the production of T3, resulting in lower TH activity in the peripheral tissues [33,34]. In the present study, we demonstrated that TH induces *MDR1* mediated by TR. Therefore, this amiodarone-induced decrease in TH activity might also lead to reduced *MDR1* expression, which indirectly inhibits P-gp mediated by TR and might serve as another pathway for amiodarone-induced P-gp inhibition.

Verapamil, another antiarrhythmic drug and well-known P-gp inhibitor, was reported to inhibit TH efflux from several cell types, suggesting that P-gp is involved in TH efflux [35,36]. Mitchell et al. demonstrated that P-gp exports thyroid hormone from cells using specific inhibitors for P-gp (verapamil, nitrendipine, VX853, and VX710) and polarized MDCKII cells stably transfected with MDR1 cDNA [37]. Together with the presently reported results, these findings suggest that the induction of *MDR1* mediated by TR might serve as a feedback regulatory mechanism for TH homeostasis. This feedback loop is as follows: the expression of P-gp is induced by TH, causing the efflux of TH from cells through the induced P-gp, resulting in lower TH content in the cells, leading to reduction in P-gp expression by the reduced TH, resulting in the accumulation of TH in the cells by the reduced P-gp, inducing P-gp expression by the accumulated TH, causing the efflux of TH from the cells by the induced P-gp, and so on.

In summary, we demonstrated that the induction of *MDR1* gene expression by TH is mediated by TR through a TH response region located between −7.9 and −7.8 kb upstream from the transcription start site of *MDR1* (Fig. 6). This region contains two closely spaced TH response clusters, one of which is designated as UpC and includes a DR3 and a DR4(I), the other of which is designated as DwC and includes two DR4s(II and III). Every direct repeat makes its own contribution to the T3 response; in particular, DR4(I) was shown to be the most important element. TR formed a heterodimer with RXR at each of the UpC, DwC, and DR motifs, with preferential binding to DR4(I) in UpC. The binding affinity to the clusters was UpC > DwC, while that to the DR motifs was DR4(I) > DR4(II) > DR3 ≈ DR4(III). These results agreed well with the relative degree of contribution to the T3 response in transcriptional activity. Two molecules of the TR/RXR heterodimer could simultaneously bind to the TH response region including UpC and DwC, although one molecule of TR/RXR bound to the region (preferentially to DR4(I)) at lower concentrations of TR/RXR. Thus, the TH response region could be equipped with a booster system that is adapted to circumstances in which a higher concentration of ligand-bound TR/RXR exists.

Acknowledgments

We thank Dr. Shuichi Koizumi (Yamanashi University) for providing the human RXRα cDNA. This work was supported in part by grants from the Ministry of Health, Labor and Welfare of Japan and the Japan Health Sciences Foundation (Research on Publicly Essential Drugs and Medical Devices).

References

[1] J.H. Lin, Adv. Drug Deliv. Rev. 55 (2003) 53–81.
[2] S. Marchetti, R. Mazzanti, J.H. Beijnen, J.H. Schellens, Oncologist 12 (2007) 927–941.
[3] F.P. Guengerich, Annu. Rev. Pharmacol. Toxicol. 39 (1999) 1–17.
[4] F.P. Guengerich, Mol. Interv. 3 (2003) 194–204.
[5] O. Burk, K.A. Arnold, A. Geick, H. Tegude, M. Eichelbaum, Biol. Chem. 386 (2005) 503–513.
[6] A. Geick, M. Eichelbaum, O. Burk, J. Biol. Chem. 276 (2001) 14581–14587.
[7] B. Goodwin, E. Hodgson, D.J. D'Costa, G.R. Robertson, C. Liddle, Mol. Pharmacol. 62 (2002) 359–365.
[8] B. Goodwin, E. Hodgson, C. Liddle, Mol. Pharmacol. 56 (1999) 1329–1339.
[9] J. Bonelli, H. Haydl, K. Hruby, G. Kaik, Int. J. Clin. Pharmacol. Biopharm. 16 (1978) 302–306.
[10] B. Greiner, M. Eichelbaum, P. Fritz, H.P. Kreichgauer, O. von Richter, J. Zundler, H.K. Kroemer, J. Clin. Invest. 104 (1999) 147–153.
[11] W. Siegmund, S. Altmannsberger, A. Paneitz, U. Hecker, M. Zschiesche, G. Franke, W. Meng, R. Warzok, E. Schroeder, B. Sperker, B. Terhaag, I. Cascorbi, H.K. Kroemer, Clin. Pharmacol. Ther. 72 (2002) 256–264.
[12] T. Mitin, L.L. Von Moltke, M.H. Court, D.J. Greenblatt, Drug Metab. Dispos. 32 (2004) 779–782.
[13] F. Flamant, J.D. Baxter, D. Forrest, S. Refetoff, H. Samuels, T.S. Scanlan, B. Vennstrom, J. Samarut, Pharmacol. Rev. 58 (2006) 705–711.
[14] M.A. Lazar, Endocr. Rev. 14 (1993) 184–193.

Please cite this article in press as: K. Kurose et al., Arch. Biochem. Biophys. (2008), doi:10.1016/j.abb.2008.03.020

[15] P.M. Yen, Physiol. Rev. 81 (2001) 1097–1142.
[16] K. Boelaert, J.A. Franklyn, J. Endocrinol. 187 (2005) 1–15.
[17] G.J. Canaris, N.R. Manowitz, G. Mayor, E.C. Ridgway, Arch. Intern. Med. 160 (2000) 526–534.
[18] M.P. Vanderpump, W.M. Tunbridge, J.M. French, D. Appleton, D. Bates, F. Clark, J. Grimley Evans, D.M. Hasan, H. Rodgers, F. Tunbridge, et al., Clin. Endocrinol. (Oxf) 43 (1995) 55–68.
[19] K. Kurose, S. Ikeda, S. Koyano, M. Tohkin, R. Hasegawa, J. Sawada, Mol. Cell. Biochem. 281 (2006) 35–43.
[20] K.E. Thummel, C. Brimer, K. Yasuda, J. Thottassery, T. Senn, Y. Lin, H. Ishizuka, E. Kharasch, J. Schuetz, E. Schuetz, Mol. Pharmacol. 60 (2001) 1399–1406.
[21] M. Jin, T. Shimada, M. Shintani, K. Yokogawa, M. Nomura, K. Miyamoto, Drug Metab. Pharmacokinet. 20 (2005) 324–330.
[22] N. Nishio, T. Katsura, K. Ashida, M. Okuda, K. Inui, Drug Metab. Dispos. 33 (2005) 1584–1587.
[23] J.M. Pascussi, S. Gerbal-Chaloin, L. Drocourt, P. Maurel, M.J. Vilarem, Biochim. Biophys. Acta 1619 (2003) 243–253.
[24] Y. Chen, G. Kissling, M. Negishi, J.A. Goldstein, J. Pharmacol. Exp. Ther. 314 (2005) 1125–1133.
[25] S. Kodama, C. Koike, M. Negishi, Y. Yamamoto, Mol. Cell. Biol. 24 (2004) 7931–7940.
[26] J. Sugatani, S. Nishitani, K. Yamakawa, K. Yoshinari, T. Sueyoshi, M. Negishi, M. Miwa, Mol. Pharmacol. 67 (2005) 845–855.
[27] E.S. Tien, M. Negishi, Xenobiotica 36 (2006) 1152–1163.
[28] T.W. Synold, I. Dussault, B.M. Forman, Nat. Med. 7 (2001) 584–590.
[29] J.M. Lehmann, D.D. McKee, M.A. Watson, T.M. Willson, J.T. Moore, S.A. Kliewer, J. Clin. Invest. 102 (1998) 1016–1023.
[30] W. Xie, M.F. Yeuh, A. Radominska-Pandya, S.P. Saini, Y. Negishi, B.S. Bottroff, G.Y. Cabrera, R.H. Tukey, R.M. Evans, Proc. Natl. Acad. Sci. USA 100 (2003) 4150–4155.
[31] J. Sugatani, H. Kojima, A. Ueda, S. Kakizaki, K. Yoshinari, Q.H. Gong, I.S. Owens, M. Negishi, T. Sueyoshi, Hepatology 33 (2001) 1232–1238.
[32] S.U. Sankatsing, J.H. Beijnen, A.H. Schinkel, J.M. Lange, J.M. Prins, Antimicrob. Agents Chemother. 48 (2004) 1073–1081.
[33] A.C. Bianco, D. Salvatore, B. Gereben, M.J. Berry, P.R. Larsen, Endocr. Rev. 23 (2002) 38–89.
[34] E. Martino, L. Bartalena, F. Bogazzi, L.E. Braverman, Endocr. Rev. 22 (2001) 240–254.
[35] F.A. Neves, R.R. Cavalieri, L.A. Simeoni, D.G. Gardner, J.D. Baxter, B.F. Scharschmidt, N. Lomri, R.C. Ribeiro, Endocrinology 143 (2002) 476–483.
[36] R.C. Ribeiro, R.R. Cavalieri, N. Lomri, C.M. Rahmaoui, J.D. Baxter, B.F. Scharschmidt, J. Biol. Chem. 271 (1996) 17147–17151.
[37] A.M. Mitchell, M. Tom, R.H. Mortimer, J. Endocrinol. 185 (2005) 93–98.

Please cite this article in press as: K. Kurose et al., Arch. Biochem. Biophys. (2008), doi:10.1016/j.abb.2008.03.020

BIOCHEMICAL PHARMACOLOGY 76 (2008) 531–542

available at www.sciencedirect.com

ScienceDirect

journal homepage: www.elsevier.com/locate/biochempharm

Identification of the functional vitamin D response elements in the human *MDR1* gene

Mayumi Saeki, Kouichi Kurose, Masahiro Tohkin, Ryuichi Hasegawa*

Division of Medicinal Safety Science, National Institute of Health Sciences, 1-18-1 Kamiyoga, Setagaya-ku, Tokyo 158-8501, Japan

ARTICLE INFO

Article history:
Received 25 March 2008
Accepted 22 May 2008

Keywords:
Multidrug resistance 1
P-glycoprotein (P-gp)
Vitamin D receptor (VDR)
1α,25-Dihydroxyvitamin D_3
Vitamin D response element (VDRE)

ABSTRACT

P-glycoprotein, encoded by the multidrug resistance 1 (*MDR1*) gene, is an efflux transporter and plays an important role in pharmacokinetics. The expression of *MDR1* is induced by a variety of compounds, of which 1α,25-dihydroxyvitamin D_3 is known to be an effective inducer. However, it remains unclear how 1α,25-dihydroxyvitamin D_3 regulates the expression of *MDR1*. In this study, we demonstrated that the vitamin D receptor (VDR) induces *MDR1* expression in a 1α,25-dihydroxyvitamin D_3-dependent manner. Luciferase assays revealed that the region between −7.9 and −7.8 kbp upstream from the transcription start site of the *MDR1* is responsible for the induction by 1α,25-dihydroxyvitamin D_3. Electrophoretic mobility shift assays revealed that several binding sites for the VDR/retinoid X receptor α (RXRα) heterodimer are located between the −7880 and −7810 bp region, to which the three molecules of VDR/RXRα are able to simultaneously bind with different affinities. Luciferase assays using mutated constructs revealed that the VDR-binding sites of DR3, DR4(I), MdC3, and DR4(III) contribute to the induction, indicating that these binding sites act as vitamin D response elements (VDREs). The contribution of each VDRE to the inducibility was different for each response element. An additive effect of the individual VDREs on induced luciferase activity by 1α,25-dihydroxyvitamin D_3 was also observed. These results indicate that the induction of *MDR1* by 1α,25-dihydroxyvitamin D_3 is mediated by VDR/RXRα binding to several VDREs located between −7880 and −7810 bp, in which every VDRE additively contributes to the 1α,25-dihydroxyvitamin D_3 response.

1. Introduction

P-glycoprotein (P-gp), which is encoded by the multidrug resistance 1 (*MDR1*) gene, transports a wide range of compounds, such as drugs and xenobiotics, from intracellular to extracellular compartments [1]. P-gp is expressed on the apical surface of epithelial cells of tissues including intestine, kidney, liver, and brain, and plays an important role in drug absorption, renal secretion, biliary excretion, and brain distribution [1]. CYP3A4 is the most abundantly expressed human cytochrome P450 contributing to drug metabolism, and P-gp and CYP3A4 share many substrates, inhibitors, inducers, and tissue distribution patterns [2]. Therefore, it has been hypothesized that the expressions of MDR1 and CYP3A4 have similar regulatory mechanisms. In fact, both genes are directly regulated by nuclear receptors, pregnane X receptor (PXR) and constitutive androstane receptor (CAR) [3–6].

Previous reports revealed that 1α,25-dihydroxyvitamin D_3 (1,25-$(OH)_2D_3$), the most active metabolite of vitamin D_3, regulates the expression of MDR1 mRNA and P-gp protein. The treatment of LS180 cells, a human colon carcinoma cell line, with 1,25-$(OH)_2D_3$ led to a significant increase in MDR1 mRNA and P-gp protein levels [7–9]. In human airway epithelium-derived Calu-3 cells, treatment with 1,25-$(OH)_2D_3$ caused

* *Corresponding author.* Tel.: +81 3 3700 9789; fax: +81 3 3700 9788.
E-mail address: kurose@nihs.go.jp (K. Kurose).
0006-2952/$ – see front matter © 2008 Elsevier Inc. All rights reserved.
doi:10.1016/j.bcp.2008.05.030

elevated P-gp expression [10]. Furthermore, Olaizola et al. reported that the uptake of [^{99m}Tc]-sestamibi (which is known to be a substrate of P-gp and is excreted by P-gp [11,12]) by the parathyroid glands of uremic patients was suppressed by pulse administration of 1,25-$(OH)_2D_3$ for 2 weeks, suggesting that P-gp induction by 1,25-$(OH)_2D_3$ leads to increased [^{99m}Tc]-sestamibi efflux [13].

The biological activity of 1,25-$(OH)_2D_3$ is mainly mediated via the vitamin D receptor (VDR), a member of the nuclear receptor superfamily. VDR forms a heterodimer with retinoid X receptor (RXR) and binds to the vitamin D response element (VDRE) in the regulatory region of genes. The VDRE by which the gene is regulated positively is generally composed of a direct repeat (DR) of the consensus hexamer (half-site) sequence of 5′-RGKTCA-3′ (R = A or G, and K = G or T) spaced by three or four nucleotides (DR3 or DR4), or an everted repeat spaced by 6, 7, 8, or 9 nucleotides (ER6, ER7, ER8, or ER9) [14–17]. However, negative response elements for 1,25-$(OH)_2D_3$ have been identified in several genes down-regulated by 1,25-$(OH)_2D_3$, such as human pituitary transcription factor-1 gene, in which an imperfect DR2 motif acts as a negative VDRE [18].

Previously, Geick et al. reported that the induction of *MDR1* by rifampin is mediated by PXR which binds to a DR4 located between −7.9 and −7.8 kbp upstream from the transcription start site [3]. Burk et al. reported that CAR also induces *MDR1* expression by binding to several DR4s located in the same region [4]. Recently, we reported that thyroid hormone receptor (TR) regulates the expression of *MDR1* by binding to several DRs located in the same region [19]. It was reported that 1,25-$(OH)_2D_3$ also regulates CYP3A4 induction through the binding of VDR/RXRα to some PXR response elements [14]. These results suggest that VDR also binds to several DR motifs in the same region of the *MDR1* gene and regulates the expression of *MDR1*. However, this theory requires substantiation.

There is variation amongst individuals in intestinal *MDR1* expression [20]. Since 1,25-$(OH)_2D_3$ induces the expression of *MDR1*, the 1,25-$(OH)_2D_3$-mediated induction process might be involved in this inter-individual variation. Furthermore, vitamin D is widely prescribed and influences the induction of P-gp, which potentially affects pharmacokinetics. Therefore, the role of vitamin D in the mechanism of *MDR1* expression is worthy of investigation. In this study, we investigated that how 1,25-$(OH)_2D_3$ regulates the expression of *MDR1* using the intestinal epithelial cell line Caco-2. We demonstrate that the induction of *MDR1* by 1,25-$(OH)_2D_3$ is mediated by VDR/RXRα binding to several VDREs located between −7880 and −7810 bp upstream of the *MDR1* gene, in which every VDRE additively contributes to the 1,25-$(OH)_2D_3$ response.

2. Materials and methods

2.1. Plasmid constructs

Human VDR cDNA was amplified from human kidney Marathon-Ready cDNA (Clontech Laboratories Inc., Palo Alto, CA, USA) with the primers 5′-ATGGAGGCAATGGCGGC-3′ and 5′-TCAGGAGATCTCATTGCCAAACAC-3′ using a TaKaRa LA Taq (Takara Bio Inc., Shiga, Japan). The resulting DNA fragment was subcloned into the pEF6/V5-His-TOPO vector (Invitrogen, Carlsbad, CA, USA) and this expression plasmid (pEF6/V5-hVDR) was used for the transfection. The sequences were verified by DNA sequencing. The pEF6/V5-hVDR plasmid was digested with KpnI (Toyobo, Osaka, Japan) and NotI (Takara Bio Inc.), and the resulting fragment was ligated into the pCMVTNT expression plasmid (Promega, Madison, WI, USA), which was digested with KpnI and NotI. This plasmid (pCMVTNT-hVDR) was used for the in vitro synthesis. The expression plasmid encoding human RXRα cDNA (pcDNA3.1-hRXRα) was a generous gift from Dr. Shuichi Koizumi (Yamanashi University, Japan). Luciferase reporter gene plasmids containing various lengths of the human *MDR1* 5′-flanking sequence were previously constructed in our laboratory [19]. Mutations in several half-sites were introduced into the pMD*824Δ90L reporter plasmid using a QuikChange Multi Site-Directed Mutagenesis kit (Stratagene, La Jolla, CA, USA) according to the manufacturer's instructions, with the previously described oligonucleotides and the following oligonucleotides, used alone or in combination: M28, 5′-GCTCCTGGGAGAGAGAACATTTGAGATTAAACAAG-3′; M31, 5′-GAACTAACTTGACCTTTTTCCTGGGAGAGAGTTC-3′; M33, 5′-AAATGAACTCAATCCCAGGAGCAAG-3′. For the M28, M29, M30, and M36 mutants shown in Fig. 4A, mutations were introduced into the M1, M3, M12, and M23 constructs using the M28 primer. For the M38 mutant shown in Fig. 4A, a deletion mutant was obtained by chance when we attempted to create the M30 mutant. All mutations were verified by DNA sequencing.

2.2. Cell culture

Caco-2 cells, a human colon adenocarcinoma cell line, were obtained from American Type Culture Collection (Manassas, VA, USA). Caco-2 cells were cultured in low glucose Dulbecco's modified Eagle's medium (DMEM, Sigma–Aldrich, St. Louis, MO, USA) supplemented with 10% heat-inactivated fetal bovine serum (FBS), 100 U/mL penicillin G/100 μg/mL streptomycin (Gibco-Invitrogen, Carlsbad, CA, USA), and 1× MEM non-essential amino acids solution (Gibco-Invitrogen) at 37 °C under 5% CO_2–95% air.

2.3. Transfection and luciferase reporter gene assays

Caco-2 cells were seeded into 96-well plates (1.6×10^4 cells/well), grown overnight, and transiently transfected using HilyMax (at a ratio of DNA to HilyMax of 1:5; Dojindo Laboratories, Kumamoto, Japan) according to the manufacturer's instructions with 10 ng/well of VDR expression plasmid (pEF6/V5-hVDR), 100 ng/well of the indicated luciferase reporter plasmid, and 10 ng/well of the *Renilla* luciferase reporter plasmid, pGL4.74 [hRluc/TK] (Promega) to normalize the transfection efficiency. After 24 h, the medium was replaced by phenol red-free DMEM (Gibco-Invitrogen) supplemented with 10% dextran-coated charcoal-stripped FBS (Hyclone Laboratories, Logan, UT, USA) containing 25 nM 1,25-$(OH)_2D_3$ (Sigma–Aldrich) or dimethyl sulfoxide (DMSO) for 3.5 h. Firefly and *Renilla* luciferase activities were measured using a Dual-Glo Luciferase Assay System (Promega) according to the manufacturer's instructions and a luminometer (Wallac 1420 ARVO sx Multilabel counter, PerkinElmer Life Sciences, Boston, MA, USA). Firefly luciferase activity was normalized to

Renilla luciferase activity, and the inducibility was calculated as the ratio of luciferase activity of 1,25-$(OH)_2D_3$-treated cells to that of control (DMSO-treated) cells. The results represent the mean ± S.D. of four independent experiments, and in each of these experiments the control and 1,25-$(OH)_2D_3$ treatments were performed at least in triplicate.

2.4. *Electrophoretic mobility shift assays (EMSAs)*

TNT T7 and SP6 Quick Coupled Transcription/Translation Systems (Promega) were used for in vitro synthesis of human RXRα protein from pcDNA3.1-hRXRα and human VDR protein from pCMVTNT-hVDR, respectively, according to the manufacturer's instructions. The plus strand sequences of probes and competitors used in EMSA are shown in Figs. 2A and 3A. The nonspecific competitor was double-stranded oligonucleotide located in the −218 to −117 region of the human PXR promoter [21]. The oligonucleotides, except for longer probes described below, were purchased from Sigma Genosys (Hokkaido, Japan) and equal amounts of complimentary strands were annealed. The longer probes, except for the 7882 probe shown in Fig. 3A, were prepared by polymerase chain reaction (PCR) amplification as described previously [19]. The reaction mixture used to obtain the results shown in Fig. 2B–D was prepared as follows: 2.5 μL aliquots of the in vitro translated proteins (VDR or RXRα alone, or mixed at a ratio of 1:1) or unprogrammed reticulocyte lysate were incubated for 20 min at room temperature with 1 μL of 5× binding buffer [15 mM $MgCl_2$, 0.5 mM EDTA, 2.5 mM dithiothreitol (DTT), 50% glycerol and 100 mM HEPES, pH 7.75], 0.5 μL of 1 mg/mL poly(dI–dC) (GE Healthcare UK Ltd., Buckinghamshire, UK), and 0.5 μL of 0.33 μM 5′-fluorescein isothiocyanate (FITC)-labeled double-stranded oligonucleotide probe. For competition assays, 0.5 μL of unlabeled oligonucleotide was simultaneously added to the reaction mixture with the probe. For the assays used to obtain the results shown in Fig. 3, 2–8 μL (Fig. 3B) or 8 μL (Fig. 3C) of the in vitro translated VDR and RXRα mixed at a ratio of 1:1 were used, if necessary, the volume of which was adjusted to 8 μL with unprogrammed reticulocyte lysate. The 8-μL aliquots of the proteins were incubated for 20 min at room temperature with 1 μL of 10× binding buffer (30 mM $MgCl_2$, 1 mM EDTA, 5 mM DTT, 50% glycerol and 200 mM HEPES, pH 7.75), 0.5 μL of 1 mg/mL poly(dI–dC), and 0.5 μL of the PCR-based probe or 0.33 μM 5′-FITC-labeled 7882 probe in the presence or absence of 250 nM 1,25-$(OH)_2D_3$. The 1.5-μL aliquots of the protein–DNA complexes were resolved by electrophoresis on 2.8 or 6% non-denaturing Long Ranger gels (Lonza, Basel, Switzerland) run in 0.5× TBE (44.5 mM Tris, 44.5 mM boric acid, and 1.25 mM EDTA) at 500 V constant voltage, and visualized and quantified on a slab gel DNA sequencer DSQ-2000L (Shimadzu Co., Kyoto, Japan).

3. Results

3.1. *Identification of the 1,25-$(OH)_2D_3$-responsive region in the MDR1 gene*

To investigate the mechanism of *MDR1* gene expression induced by 1,25-$(OH)_2D_3$, we performed a luciferase reporter gene assay using an intestinal epithelial cell line, Caco-2, which expresses VDR at relatively lower level [9]. The cells were transfected with a reporter plasmid containing the 5′-upstream region from −10082 to +117 bp of *MDR1* (pMD10082L) in the presence or absence of an expression plasmid encoding VDR. Following the treatment with either vehicle (DMSO) or 1,25-$(OH)_2D_3$, luciferase assays were performed. In the absence of VDR expression plasmid, 1,25-$(OH)_2D_3$ had little affect on the transcriptional activity. By contrast, in the presence of VDR expression plasmid, more than an eightfold activation was induced by 1,25-$(OH)_2D_3$ (Fig. 1A). These results indicate that the 1,25-$(OH)_2D_3$-responsive region is located within 10 kbp of the 5′-flanking region of *MDR1*, and that VDR mediates *MDR1* induction by 1,25-$(OH)_2D_3$.

Next, to identify the response elements implicated in the transcriptional regulation of *MDR1* by 1,25-$(OH)_2D_3$, we performed luciferase assays using several deletion mutants of pMD10082L. As shown in Fig. 1A, the 824 bp deletion from −7970 to −7145 bp resulted in the complete loss of inducibility. The lost inducibility was recovered by reinsertion of the deleted region of 824 bp (Fig. 1A, bottom line, pMD*824L). These results indicate that the 824 bp region is essential for the induction of *MDR1* by 1,25-$(OH)_2D_3$.

To further define the minimal region for the VDR response, deletion analysis was performed based on pMD*824L, which contains the 824 bp region (Fig. 1B). The 90 bp deletion from the 5′-end did not affect inducibility, whereas the 153 bp deletion from the 5′-end resulted in the complete loss of inducibility. These data suggest that the essential region for the VDR-mediated induction is located between −7880 and −7817 bp.

3.2. *VDR binds to the putative VDRE as a heterodimer with RXRα*

We scanned the 1,25-$(OH)_2D_3$ response region between −7880 and −7810 bp using the JASPAR FAM database (http://jaspar.genereg.net/). Several putative half-sites, a pair of which composes a DR or ER, were found (Hs1–8, Fig. 2A). Generally, some DRs or ERs, including DR3 and DR4 (which lie in this region, as shown in Fig. 2A) act as VDRE.

The region including the putative VDRE was divided into three segments, designated upstream cluster (UpC), middle cluster (MdC), and downstream cluster (DwC); we have reported this convenient classification previously [19]. Each cluster has several putative half-sites. To determine whether VDR and RXRα could bind directly to these segments, EMSA was performed using in vitro translated VDR and RXRα. The probes and competitors used for the EMSA are summarized in Fig. 2A. The DNA–protein complexes were formed in the presence of both VDR and RXRα, although the complexes were not formed in the absence of either protein, indicating that the protein complex VDR/RXRα binds to each segment (Fig. 2B–D). The DNA–protein complexes were competed out by the self-competitors but were not competed out by the nonspecific competitor (Fig. 2B–D). The relative affinities of VDR/RXRα to UpC, MdC, and DwC were further assessed by competition experiments. As shown in Fig. 2B, the complexes of UpC with VDR/RXRα were competed out by competitors UpC, MdC, and DwC. Of these, UpC was the most effective competitor for the formation of the DNA–protein complexes, and MdC inhibited

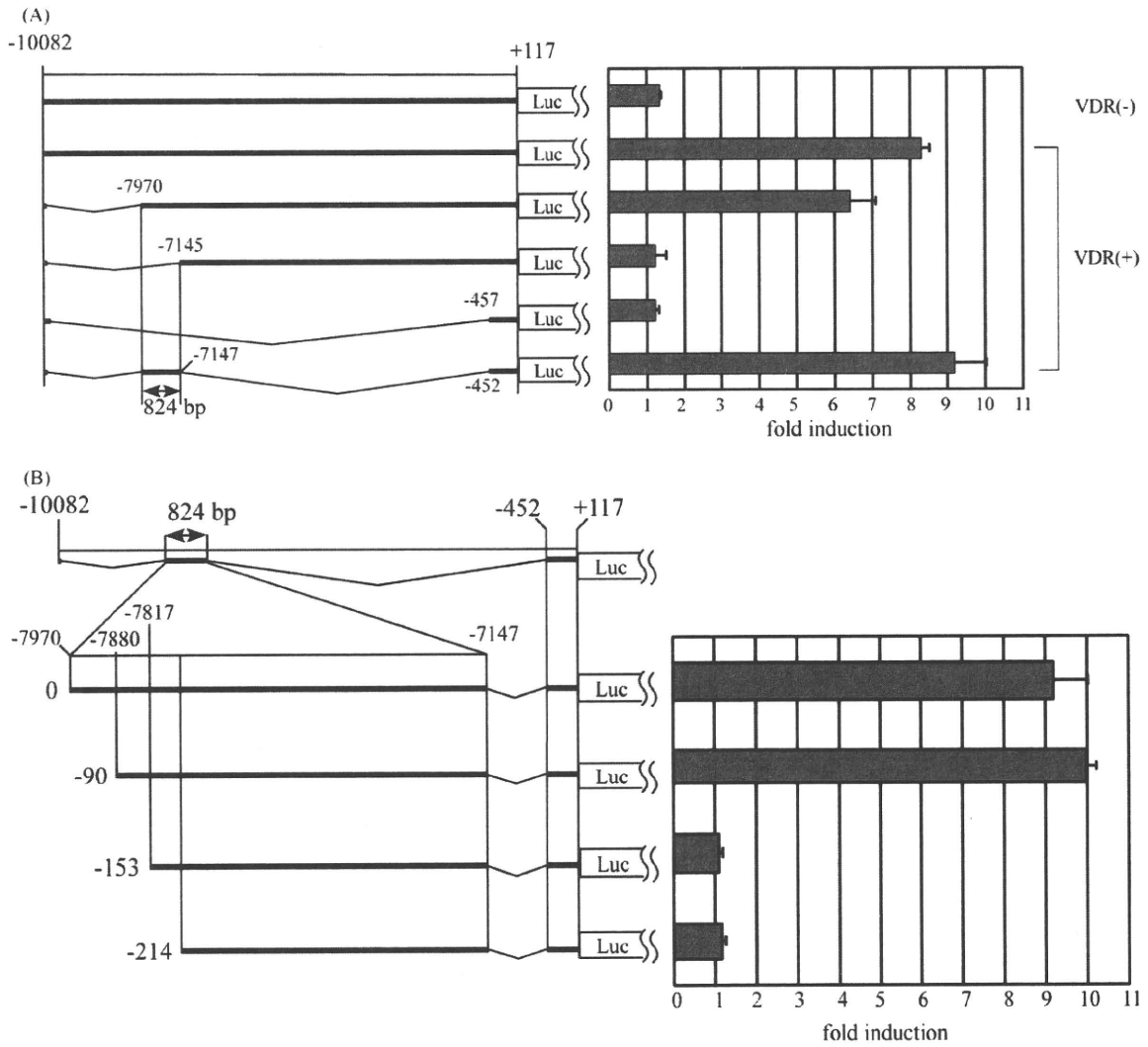

Fig. 1 – Transcriptional activity of several deletion mutants of human *MDR1* in the 5′-upstream region induced by 1,25-$(OH)_2D_3$. The 5′-upstream region of the *MDR1* gene was cloned into pGL4.12, as indicated on the left. Numbers are in reference to the transcriptional start site at +1. Luciferase activity was analyzed as described in Section 2. Fold induction was calculated as the ratio of luciferase activity in 1,25-$(OH)_2D_3$-treated cells to that of DMSO-treated cells, and is indicated on the right side of each column. Each value represents the mean ± S.D. of four independent experiments. (A) Schematic representations of pMD10082L, pMD7970L, pMD7145L, pMD457L and pMD*824L are shown from the top of the left side. (B) Schematic representations of pMD*824L, pMD*824Δ90L, pMD*824Δ153L, and pMD*824Δ214L are shown from the top of the left side.

complex formation to an extent similar to that of DwC (Fig. 2B). Similar competition assay results were obtained using MdC and DwC probes (Fig. 2C and D).

To identify the VDR/RXRα-binding site in these segments, shorter oligonucleotides containing two or three half-sites were used as competitors (Fig. 2B). The most efficient competitor for VDR/RXRα binding to UpC was DR4(I), followed by DR3, MdC3, DR4(III), and DR4(II). MdC5 lacking Hs6 of MdC was not able to compete for the UpC probe, indicating that Hs6 is necessary for MdC–VDR/RXRα binding.

Next, oligonucleotides including a set of 2 bp mutations in each of the half-sites (UpM1~DwM12 in Fig. 2A) were used as competitors for EMSA. As shown in Fig. 2B, UpM1 including the Hs1 mutation in UpC competed for the UpC probe at the same level as the wild-type competitor. UpM3 including the Hs3 mutation in UpC competed slightly less efficiently than the wild-type. UpM2 including the Hs2 mutation in UpC failed to compete for UpC, indicating that Hs2 is essential for UpC–VDR/RXRα complex formation (Fig. 2B).

The result obtained using the MdC probe is shown in Fig. 2C. To determine which half-site of MdC3 is required for MdC–VDR/RXRα complex formation, the mutant oligonucleotides including the 2 bp mutations in the half-sites of MdC3 were used as competitors (MdM31, M33, and M4). MdM31 including the Hs4 mutation partially competed for MdC, but MdM33 containing the Hs5 mutation competed for MdC as effectively as the wild-type competitor. MdM4 including the Hs6 mutation in MdC3 failed to compete for

the MdC probe, indicating that Hs6 is essential for MdC3–VDR/RXRα complex formation. This result is consistent with the fact that MdC5, which lacks Hs6 of MdC, is not able to bind VDR/RXRα.

The result obtained using the DwC probe is shown in Fig. 2D. The Hs6 and Hs7 mutations in DwC (DwM4 and DwM7, respectively) did not affect the competition for DwC, whereas the Hs8 mutation caused reduced competition by DwM12 for

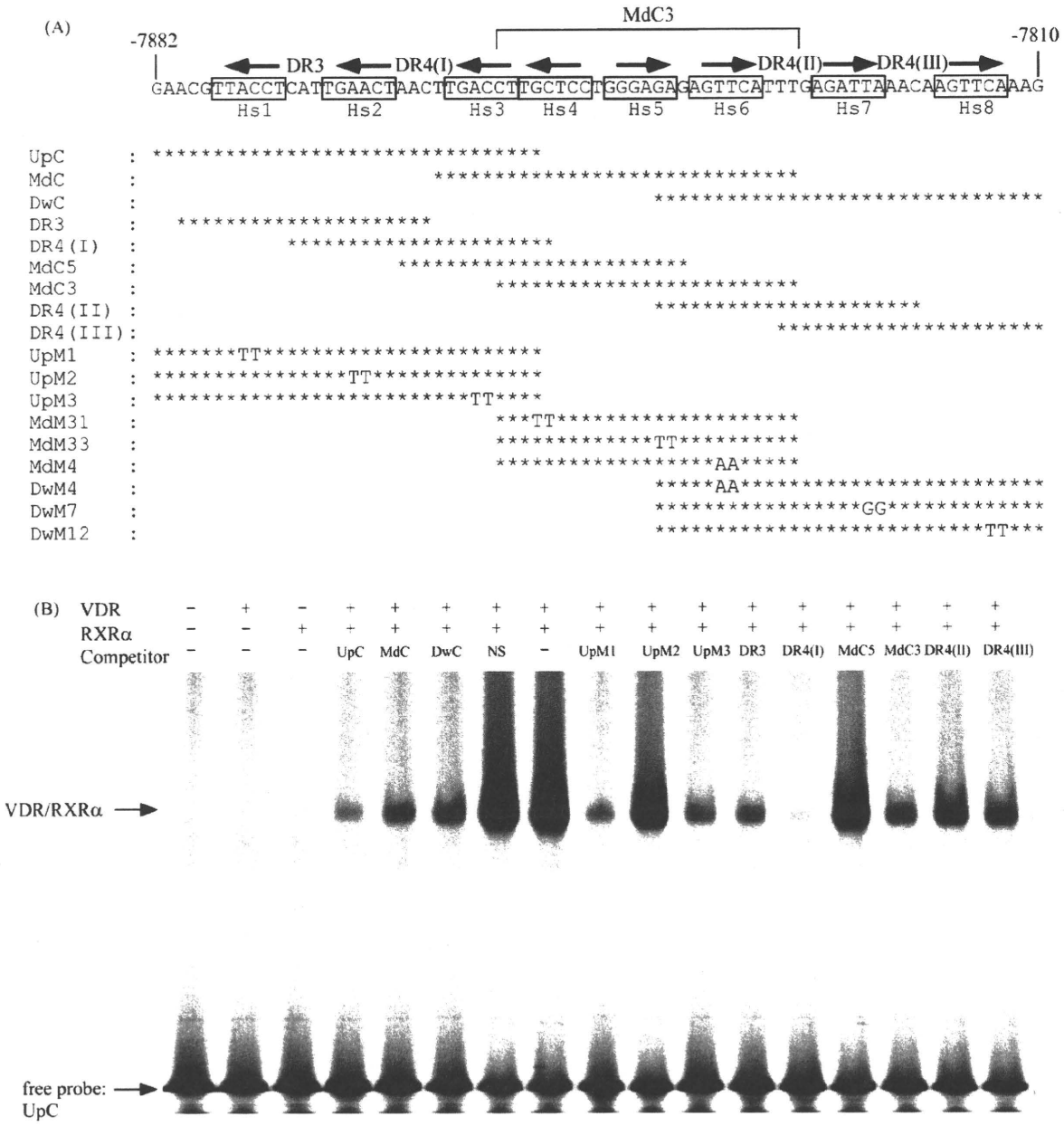

Fig. 2 – VDR binds to the putative VDREs in the region essential for VDR-mediated induction as a heterodimer with RXRα. (A) Oligonucleotide sequences used for EMSA. Putative half-sites (Hs1–8) predicted using JASPAR FAM are boxed, and arrows indicate the direction of the half-site. Numbers are in reference to the transcriptional start site at +1. Only nucleotides that differ from the wild-type are shown as letters; asterisks represent unchanged nucleotides. (B) EMSA was performed using a FITC-labeled UpC probe. The UpC probe was incubated in the absence or presence of in vitro translated VDR, RXRα, or both proteins, as described in Section 2. In parallel experiments, a competition assay was performed in the presence of a 50-fold molar excess of unlabeled oligonucleotide. "NS" indicates nonspecific competitor. The complexes were resolved by electrophoresis on a 6% Long Ranger gel. (C) EMSA was performed using a FITC-labeled MdC probe. The procedure was the same as that described in (B), except that a 15-fold molar excess of unlabeled oligonucleotides were used for the competition assay. "NS" indicates nonspecific competitor. (D) EMSA was performed using a FITC-labeled DwC probe. The procedure was the same as that described in (C). "NS" indicates nonspecific competitor.

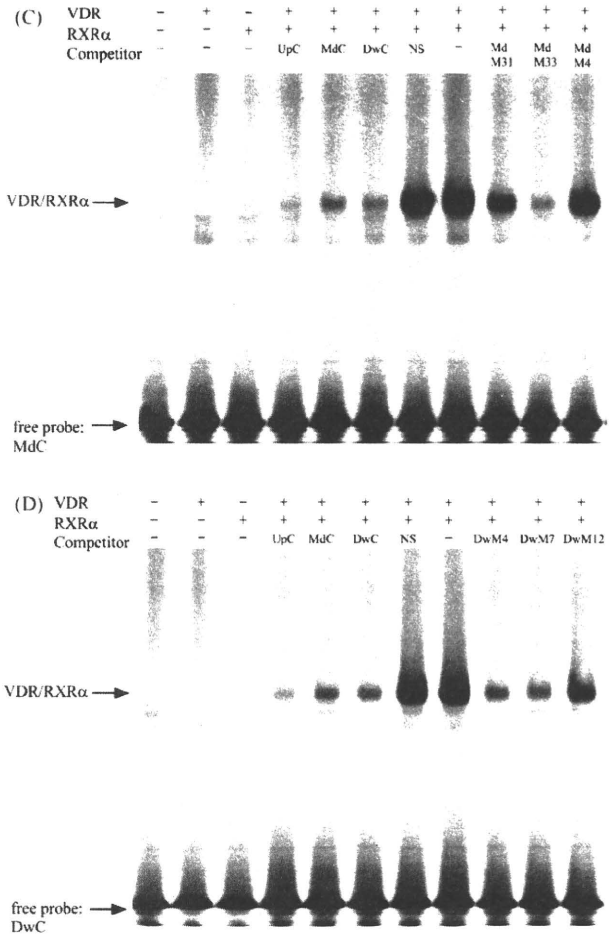

Fig. 2. (Continued).

the DwC probe. These results indicate that Hs8 is important for DwC–VDR/RXRα complex formation.

Taken together, VDR/RXRα is able to bind to several putative VDREs [DR4(I) and DR3 in UpC, MdC3 in MdC, and DR4(III) and DR4(II) in DwC] with different affinity. Additionally, Hs2, Hs6, and Hs8 are the most important half-sites in each segment for DNA–VDR/RXRα complex formation.

3.3. *Three molecules of VDR/RXRα are able to bind to the VDR-binding region at the same time*

Although we identified several sites competent to bind VDR/RXRα, the sites in this region are spaced relatively close to each other. The proximity of these VDR-binding sites might prevent the binding of VDR/RXRα to these sites. Therefore, the question that arises is how many molecules of VDR/RXRα bind to the VDR-binding region at the same time. To examine this, we performed EMSA using a longer probe (7882 probe in Fig. 3A) containing all the half-sites of the VDR-binding elements using different amounts of VDR/RXRα. At the highest concentration of the protein in the presence of 1,25-$(OH)_2D_3$, three shifted bands (upper, middle, and lower) were observed, although the intensity of the upper mobility band (3× VDR/RXRα in Fig. 3B) was weak. In the absence of 1,25-$(OH)_2D_3$, the upper band was very weak. The mobility of the lower band (1× VDR/RXRα in Fig. 3B) is the same as that of bands formed by UpC and DR4(II) probes (data not shown), to which one molecule of VDR/RXRα binds. This indicates that the lower band is the complex formed by the probe binding to one molecule of VDR/RXRα. As the amount of the protein was decreased, the intensity of the middle band (2× VDR/RXRα in Fig. 3B) decreased, while the intensity of the lower band remained constant. These results suggest that the middle band is the complex formed by the probe and two molecules of VDR/RXRα, and that three molecules of VDR/RXRα bind to this region with different affinities.

Furthermore, we performed EMSA in the presence of 1,25-$(OH)_2D_3$, which was required for the observation of three shifted bands (Fig. 3B), using longer probes containing at least one mutated half-site (Hs2, Hs6, and/or Hs8). These sites were shown to play an important role in DNA–VDR/RXRα complex formation in each segment, as shown in Fig. 2. The probes used for the EMSA are summarized in Fig. 3A. As shown in Fig. 3C, the upper bands in Fig. 3B disappeared when the M2, M4, and M12 probes were used; these probes each have one mutated half-site. In contrast, the M22, M23, and M30 probes, in which two of the three half-sites were mutated, caused the middle bands to disappear in addition to the upper bands.